Tagged EMC Measurements on Light Nuclei

W. R. Armstrong, J Arrington, I. Cloët, K. Hafidi[†], M. Hattawy, D. Potteveld, P. Reimer, Seamus Riordan, Z. Yi

Argonne National Laboratory, Lemont, IL 60439, USA

J. Ball, M. Defurne, M. Garçon, H. Moutarde, S. Procureur, F. Sabatié

CEA, Centre de Saclay, Irfu/Service de Physique Nucléaire, 91191 Gif-sur-Yvette, France

W. Cosyn

Department of Physics and Astronomy, Proeftuinstraat 86, Ghent University, 9000 Ghent, Belgium

M. Mazouz

Faculté des Sciences de Monastir, 5000 Tunisia

A. Accardi

Hampton University, Hampton, VA 23668, USA

J. Bettane, R. Dupré[†‡], M. Guidal, D. Marchand, C. Muñoz, S. Niccolai, E. Voutier

Institut de Physique Nucléaire, CNRS-IN2P3, Univ. Paris-Sud, Université Paris-Saclay, 91406 Orsay Cedex, France

K. P. Adhikari, J. A. Dunne, D. Dutta, L. El Fassi, L. Ye

Mississippi State University, Mississippi State, MS 39762, USA

M. Amaryan, G. Charles[†], G. Dodge

Old Dominion University, Norfolk, VA 23529, USA

V. Guzey

Petersburg Nuclear Physics Institute, National Research Center "Kurchatov Institute",

arXiv:1708.00891v1 [nucl-ex] 2 Aug 2017

[†]Spokesperson

[‡]Contact person: dupre@ipno.in2p3.fr

Gatchina, 188300, Russia

N. Baltzell[†], F. X. Girod, C. Keppel, S. Stepanyan
Thomas Jefferson National Accelerator Facility, Newport News, VA 23606, USA

B. Duran, S. Joosten, Z.-E. Meziani, M. Paolone, M. Rehfuss, N. Sparveris
Temple University, Philadelphia, PA 19122, USA

F. Cao, K. Joo, A. Kim, N. Markov
University of Connecticut, Storrs, CT 06269, USA

C. Ciofi degli Atti, S. Scopetta
Università di Perugia, INFN, Italy

W. Brooks, A. El-Alaoui
Universidad Técnica Federico Santa María, Valparaíso, Chile

S. Liuti
University of Virginia, Charlottesville, VA 22903, USA

a CLAS Collaboration Proposal

Nuclear Exclusive and Semi-inclusive Measurements with a New CLAS12 Low Energy Recoil Tracker

ALERT Run Group[†]

EXECUTIVE SUMMARY

In this run group, we propose a comprehensive physics program to investigate the fundamental structure of the ^{4}He nucleus. An important focus of this program is on the coherent exclusive Deep Virtual Compton Scattering (DVCS) and Deep Virtual Meson Production (DVMP) with emphasis on ϕ meson production. These are particularly powerful tools enabling model-independent nuclear 3D tomography through the access of partons' position in the transverse plane. These exclusive measurements will give the chance to compare directly the quark and gluon radii of the helium nucleus. Another important measurement proposed in this program is the study of the partonic structure of bound nucleons. To this end, we propose next generation nuclear measurements in which low energy recoil nuclei are detected. The tagging of recoil nuclei in deep inelastic reactions is a powerful technique, which will provide unique information about the nature of medium modifications through the measurement of the EMC ratio and its dependence on the nucleon off-shellness. Finally, we propose to measure incoherent spectator-tagged DVCS on light nuclei (d, ^{4}He) where the observables are sensitive to the Generalized Parton Distributions (GPDs) of a quasi-free neutron for the case of the deuteron, and bound proton and neutron for the case of ^{4}He. The objective is to study and separate nuclear effects and their manifestation in GPDs. The fully exclusive kinematics provide a novel approach for studying final state interactions in the measurements of the beam spin asymmetries and the off-forward EMC ratio.

At the heart of this program is the Low Energy Recoil Tracker (ALERT) combined with the CLAS12 detector. The ALERT detector is composed of a stereo drift chamber for track reconstruction and an array of scintillators for particle identification. Coupling these two types of fast detectors will allow ALERT to be included in the trigger for efficient

---

[†]Contact Person: Kawtar Hafidi (kawtar@anl.gov)

background rejection, while keeping the material budget as low as possible for low energy particle detection. ALERT will be installed inside the solenoid magnet instead of the CLAS12 Silicon Vertex Tracker and Micromegas tracker. We will use an 11 GeV longitudinally polarized electron beam (80% polarization) of up to 1000 nA on a gas target straw filled with deuterium or ^{4}He at 3 atm to obtain a luminosity up to 6×10^{34} nucleon cm^{-2}s^{-1}. In addition we will need to run hydrogen and ^{4}He targets at different beam energies for detector calibration. The following table summarizes our beam time request:

Configurations	Proposals	Targets	Beam time request	Beam current	Luminosity*
			days	nA	n/cm^2/s
Commissioning	All†	^{1}H, ^{4}He	5	Various	Various
A	Nuclear GPDs	^{4}He	10	1000	6×10^{34}
B	Tagged EMC & DVCS	^{2}H	20	500	3×10^{34}
C	All†	^{4}He	20	500	3×10^{34}
TOTAL			**55**		

---

*This luminosity value is based on the effective part of the target. When accounting for the target's windows, which are outside of the ALERT detector, it is increased by 60%.

†"All" includes the four proposals of the run group: Nuclear GPDs, Tagged EMC, Tagged DVCS and Extra Topics. Note that the beam time request is only driven by the three first proposals.

Abstract

We propose to measure tagged deep inelastic scattering from light nuclei (deuterium and ^{4}He) by detecting the low energy nuclear spectator recoil (p, ^{3}H and ^{3}He) in addition to the scattered electron. The proposed experiment will provide stringent tests leading to clear differentiation between the many models describing the EMC effect, by accessing the bound nucleon virtuality through its initial momentum at the point of interaction. Indeed, conventional nuclear physics explanations of the EMC effect mainly based on Fermi motion and binding effects yield very different predictions than more exotic scenarios, where bound nucleons basically loose their identity when embedded in the nuclear medium. By distinguishing events where the interacting nucleon was slow, as described by a mean field scenario, or fast, very likely belonging to a correlated pair, will clearly indicate which phenomenon is relevant to explain the EMC effect. An important challenge for such measurements using nuclear spectators is the control of the theoretical framework and, in particular, final state interactions. This experiment will directly provide the necessary data needed to test our understanding of spectator tagging and final state interactions in ^{2}H and ^{4}He and their impact on the semi-inclusive measurements of the EMC effect described above.

Contents

Introduction

Inclusive electron scattering is a simple and yet a powerful tool to probe the structure of the nucleus; in the Deep Inelastic Scattering (DIS) regime it allows to access the partonic structure of hadrons. Using the nucleus as a target permits to study how nucleons and their parton distributions are modified when embedded in the nuclear environment. The modification of quark distributions in bound nucleons was first observed through the modification of the per-nucleon cross section in nuclei, known as the "EMC effect" [1]. For moderate Bjorken x, $0.35 \leqslant x_B \leqslant 0.7$, the per-nucleon DIS structure function for nuclei with A $\geqslant 3$ was found to be suppressed compared to that of deuterium, the historic measurement being confirmed and refined in the past 30 years [2, 3, 4, 5, 6, 7].

Since its discovery, the EMC effect has been a subject of extensive theoretical investigations aimed at understanding its underlying physics. While progress has been made in interpreting the main features of the effect, no single model has been able to explain convincingly the effect for both its x_B and A dependencies [8, 9, 10]. A unifying understanding of the physical picture is still under intense debate. Most models of the EMC effect can be classified into two main categories:

- "Conventional" nuclear models [11, 12, 13, 14] in which the effect could be understood by a reduced effective nucleon mass due to the nuclear binding, causing a shift of x_B to higher values (x_B-rescaling or binding models). In these models the mass shift is sometimes accompanied by an increased density of virtual pions associated with the nuclear force (pion cloud models).

- Models involving the change of the quark confinement size in the nuclear medium [15, 16, 17, 18] can be viewed, in the language of QCD, as Q^2 rescaling models. In some cases, a simple increase of the nucleon radius is assumed (nucleon swelling), while in others, quark deconfinement is invoked and the nucleon degrees of freedom are replaced by multi-quark clusters.

- Some more elaborate models fall in between or give very different predictions. We note here in particular the Point Like Configurations (PLC) suppression model as it gives direct predictions as a function of the nucleon off-shellness. It was argued in [19] that PLCs are suppressed in bound nucleons and that large x_B configurations in nucleons have smaller than average size leading to the EMC effect at large x_B. The EMC effect
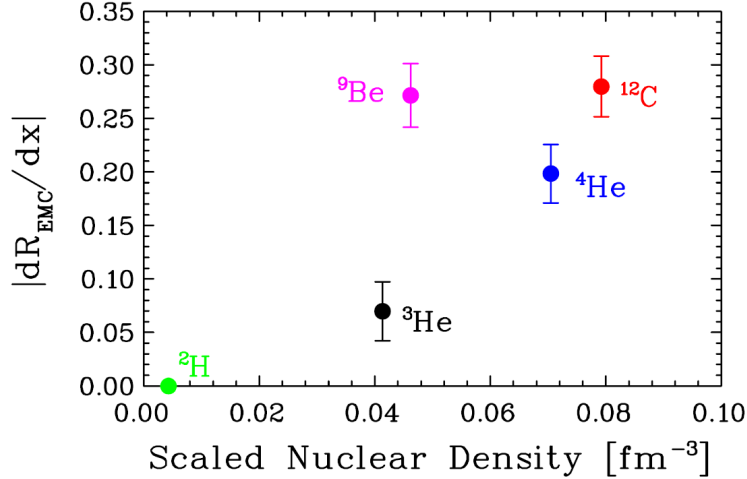
Figure 1: The slope of the isoscalar EMC ratio (*i.e.* the EMC ratio corrected for isospin asymmetry) for $0.35 < x_B < 0.7$ as a function of nuclear density [7].

in this model is predicted to be proportional to the off-shellness of the struck nucleon and hence dominated by the contribution of the short-range correlations.

Recent experiment at Jefferson Lab measured the EMC effect for a series of light nuclei [7] changing significantly our understanding of the EMC effect. The ^{3}He EMC ratio was found to be roughly one third of the effect observed in ^{4}He, violating the A-dependent fit to the SLAC data. Similarly, the density-dependent description of the EMC effect has been contradicted by the large EMC effect found in ^{9}Be (Figure 1). This suggests that the EMC effect may be sensitive to the local density experienced by a given nucleon or details of the nuclear structure, which has been first suggested in [20]. Other models have also predicted a local EMC effect and describe the modification of the nucleons depending on their shells [21, 22, 23]. The possibility of the EMC effect depending on the local environment of the nucleon also motivates the investigation of possible connections between the EMC effect and other density-dependent effects such as nucleon short-range correlations [24, 25].

Short-range correlations (SRC) occur between nucleons located at less than the average inter-nucleon distance with high relative momentum [27, 28, 29]. Those pairs of nucleons carry 80% of all nucleons kinetic energy inside the nucleus although they only represent about 20% of the total number of nucleons [30]. The plateau obtained in the inclusive cross section ratios of two nuclei (for example iron and deuterium) in the region $x_B > 1.5$ for $Q^2 > 1.5$ GeV^2 indicates that for nucleon momentum larger than Fermi momentum ($p \geqslant p_N \simeq 275$ MeV/c), the nucleon momentum distributions in different nuclei have similar shapes but differ in magnitude. The ratio of the cross sections in the plateau region also called the "SRC scale factor $a_{2N}(A/d)$" was found to be linearly correlated with the slope of the EMC effect [25]. This striking correlation shown in Figure 2
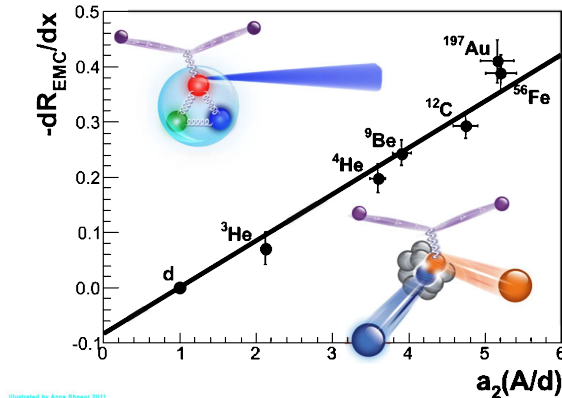
Figure 2: The EMC slopes versus the SRC scale factors from [26]. The uncertainties include both statistical and systematic errors added in quadrature.

could indicate that high momentum bound nucleons are important players in the EMC effect.

To investigate the EMC effect further, we need to find ways of looking into the nuclei with a sensitivity to the local density experienced by the nucleon we probe. This is possible by measuring the recoil fragment of the nucleus in addition to the scattered electron. Similarly to the SRC, the momentum of the recoil gives indications on the inter nucleon distance at the time of the interaction. Moreover, the momentum of this recoil can be linked to the off-shellness of the interacting nucleon [31] opening new avenues to understand how the EMC effect arise in the nucleus. The two main challenges to perform such a measurement are, first, to be able to detect the low energy nuclear fragments and, second, to understand the Final State Interaction (FSI) effects on the observables.

The recent development of two small radial time projection chambers (RTPC) by the CLAS collaboration for the measurement of the structure function of the neutron, by tagging the spectator proton from a deuterium target [32], and the measurement of coherent deep virtual Compton scattering off ^{4}He [33] has raised a lot of interest to use the same detector for this proposed tagged EMC measurement. However, it was found that the particle identification capabilities of the RTPC are not good enough to properly distinguish the different nuclear isotopes measured (in particular ^{3}H from ^{3}He). Therefore, we propose to use a different detector (a Low Energy Recoil Tracker - ALERT) based on a low gain drift chamber and a scintillator array for time of flight measurements. Such a detector appears to be perfectly suited for our measurement as it offers low energy and large angle capabilities to measure slow recoils similar to the RTPC. Moreover, such a detector will be much faster to collect the deposited charges making it possible to include it in the trigger. This will allow to ignore the overwhelming majority of the events ($\sim 90\%$) where the nuclear recoil does not make it into the detection area and reduce the pressure on the DAQ.

Another important challenge for tagged measurements is to control the impact of FSI on the observables. The large acceptance of both CLAS12 and ALERT is very important in this regard as it allows to measure at the same time the regions of the phase space expected to have negligible FSI and the regions where we expect a larger FSI effect. The models used to correct for FSI [34, 35, 36, 37] can therefore be tested in a wide kinematic range in the exact same conditions as the main measurement in order to ensure that the effect is understood properly. Then with the application of cuts to select the region where the effect is small, we can reduce the impact of FSI to a minimum. This procedure allows to make sure FSI effects are small and under control to minimize systematic uncertainty on our observables.

Chapter 1

The EMC effect in SIDIS

At this point, it became clear that in order to advance our understanding of the EMC effect, it is necessary to study it as a function of new kinematic variables such as the nucleon off-shellness, which is accessible in semi inclusive measurements. Interests for slow nucleons and fragments tagging $(e + A \rightarrow e' + N + X)$ studies are older than the EMC effect itself and has been identified earlier to be a promising tool to study nuclear effects [20, 38, 39]. In more recent work, Melnitchouk *et al.* [40] showed that the tagged structure functions of deuteron in $(e, e'N_s)$ semi-inclusive reactions, where N_s denotes the spectator nucleon, is a sensitive probe of the modification of the intrinsic structure of the bound nucleon allowing to discriminate between different EMC models. The extended case to heavier nuclei A, where the recoil nucleus $(A - 1)$ is tagged was developed by Ciofi degli Atti *et al.* [23, 37, 41, 42], highlighting the importance of such measurements in the understanding the EMC effects. In this proposal, we want to investigate the origin of the medium induced modification of the nucleon structure function through several observables based on tagged DIS off deuterium and helium targets.

1.1 The spectator mechanism

In the spectator mechanism or plane wave impulse approximation (PWIA), the DIS process corresponds to the absorption of the virtual photon by a quark inside a nucleon, followed by the recoil of the spectator nucleus $A - 1$ without any final state interaction (Figure 1.1). The differential semi-inclusive cross section can be written as [23]

$$\sigma_1^A(x_B, Q^2, \vec{P}_{A-1}, y_A, z_1^A) = \frac{d^4\sigma}{dx dQ^2 d\vec{P}_{A-1}} = K^A(x, y_A, Q^2, z_1^A) n_A(|\vec{P}_{A-1}|) z_1^A F_2^{N/A}(x_A, Q^2, p_1^2),$$

$$(1.1)$$

where $Q^2 = -q^2 = -(k_e - k_e')^2 = \vec{q}^2 - \nu$ is the four-momentum transfer, with $\vec{q} = \vec{k_e} - \vec{k_e'}$ and $\nu = E_e - E_e'$, $x_B = Q^2/2M\nu$ is the Bjorken scaling variable, $p_1 \equiv (p_{10}, \vec{p_1})$, with $\vec{p_1} \equiv -\vec{P}_{A-1}$, is the four-momentum of the off-shell nucleon before its interaction with the virtual photon.
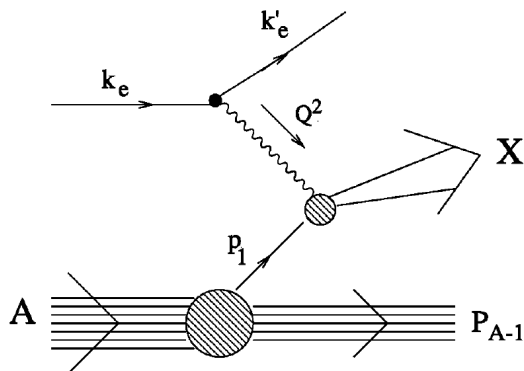
Figure 1.1: The process $A(e, e'(A-1))X$ within the impulse approximation [23].

$F_2^{N/A}$ is the DIS structure function of the nucleon N in the nucleus A, $n_A(|\vec{P}_{A-1}|)$ is the three-momentum distribution of the bound nucleon, $z_1^A = (p_1 \cdot q)/M\nu$ is the light cone momentum of the bound nucleon and K^A is a kinematical factor given by

$$K^A(x_B, y_A, Q^2, z_1^A) = \frac{4\pi\alpha^2}{Q^4 x_B} \cdot \left(\frac{y}{y_A}\right)^2 \times \left(\frac{y_A^2}{2} + (1 - y_A) - \frac{p_1^2 x_B^2 y_A^2}{(z_1^A)^2 Q^2}\right), \qquad (1.2)$$

with $y = \nu/E_e$, $y_A = (p_1 \cdot q)/(p_1 \cdot k_e)$ and $x_A = x_B/z_1^A$.

Nuclear effects in Eq. 1.1 are generated by the nucleon momentum distribution $n_A(|\vec{P}_{A-1}|)$ and by the quantities y_A and z_1^A, which differ from the corresponding quantities for a free nucleon ($y = \nu/E_e$ and $z_1^N = 1$). In this framework the off-mass shellness of the nucleon ($p_1^2 \neq M^2$) generated by nuclear binding is taken into account within some small relativistic corrections when $A > 2$ [43]. In all the studies we propose here, it is important to ensure that the spectator mechanism is dominant and that scattering between spectator nucleons and other reaction products is properly modeled. Our main goal here is to make sure we understand the simple deuterium case as well as the more complex helium target.

To test the spectator mechanism, we use the $\vec{P}_{A-1}$ dependence of semi-inclusive cross section ratio of different nuclei at the same values of x_B, Q^2 and with $|\vec{P}_{A'-1}| = |\vec{P}_{A-1}|$

$$R(x_B, Q^2, |\vec{P}_{A-1}|, z_1^A, z_1^{A'}, y_A, y_{A'}) \equiv \frac{\sigma_1^A(x_B, Q^2, |\vec{P}_{A-1}|, z_1^A, y_A)}{\sigma_1^{A'}(x_B, Q^2, |\vec{P}_{A'-1}|, z_1^{A'}, y_{A'})}. \qquad (1.3)$$

In the Bjorken limit, the A dependence of R is expected to be entirely dominated by the nucleon momentum distribution $n_A(|\vec{P}_{A-1}|)$, which exhibits a strong A dependence. Therefore, measurements of the R ratio as a function of the recoil momentum $|\vec{P}_{A-1}|$ provide a strong test of the spectator mechanism independently of the model for $F_2^{N/A}$. Figure 1.2
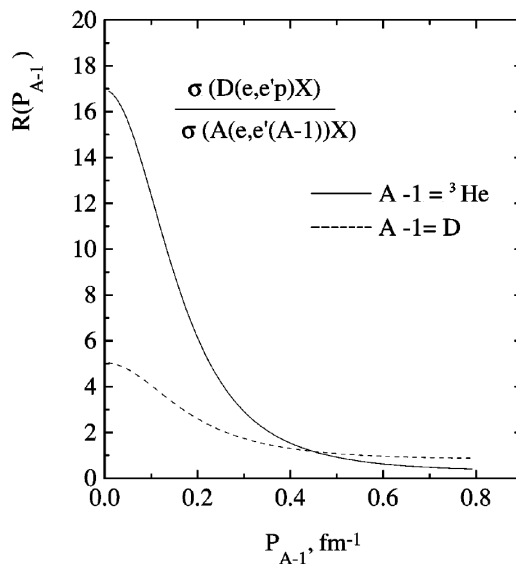
Figure 1.2: The ratio $R(A, A', |\vec{P}_{A-1}|)$ for the targets ^{3}H (dashed) and ^{4}He (full) as a function of the momentum of the backward emitted nucleus [23] relative to the virtual photon direction.

illustrates the expected behavior of the ratio in Eq. 1.3 from the processes $D(e, e'p)X$, ^{3}He$(e, e'D)X$ and ^{4}He$(e, e'^3$He$)X$, as deep inelastic scattering off a bound neutron in different nuclei.

Detailed studies [34, 35, 36, 37, 40, 44, 45] have shown that the FSI effects are minimized in the backward recoiling angle relative to the virtual photon direction and maximized in perpendicular kinematics. From the previous discussion, it is clear that the observation of recoiling nuclei in the ground state, with a $|\vec{P}_{A-1}|$-dependence similar to the one predicted by the momentum distributions, would confirm these studies and the absence of significant FSI between the electroproduced hadronic states and the nuclear fragments.

1.2 EMC effect in deuteron

Recent work from Griffioen *et al.* [46] has shown that the EMC effect is present, but very small, in the deuteron. However, the recent finding of the possible dependence of the EMC effect on local nuclear density raised the interest in using spectator nucleons to study the EMC effect. Indeed, the momentum of the spectator nucleon can be directly linked to the distance between the two nucleons in the deuteron [43] and therefore results in the enhancement of the EMC effect in certain configurations.
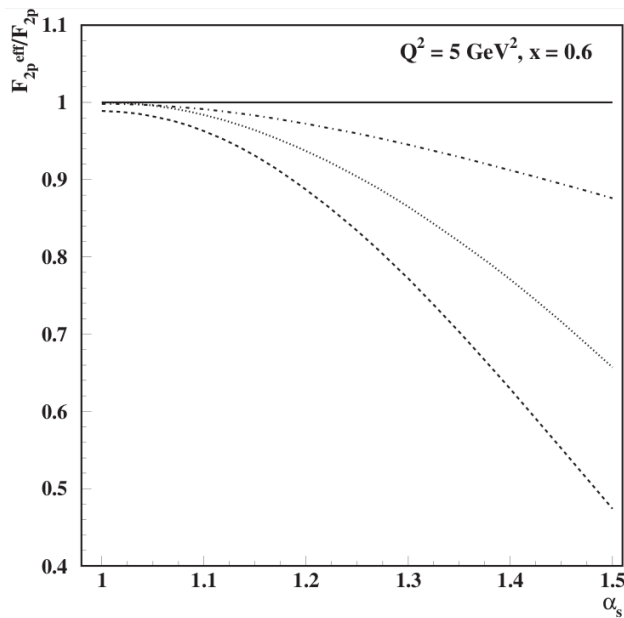
Figure 1.3: F_{2p}^{eff} as a function of α_s for $x = 0.6$ and $p_T = 0$. Dashed line is a prediction for the PLC suppression model, dotted is for the Q^2-rescaling model, and dot-dashed for the binding/off-shell model [40].

Melnitchouk *et al.* [40] use the ratio of the effective F_{2p}^{eff} measured in the deuterium, tagging the neutron, and compare it to the usual free F_{2p}. They predict significant effects for various models as a function of $\alpha \equiv \dfrac{E_s - p_z^s}{M}$ (with E_s and p_z^s the energy and longitudinal momentum of the spectator, respectively, and M its mass), which characterizes the nucleon off-shellness. A semi-inclusive measurement will allow to discriminate between the very different model predictions (Figure 1.3).

1.3 EMC effect in helium

The process described for deuterium can be easily extended to heavier nuclei with several advantages. First, the nuclear effects in light nuclei, such as ^{4}He, are much stronger, thus it enhances significantly the cross section for events with spectator momentum $\gtrsim 250$ MeV. Second, by detecting an intact light nucleus (^{3}H or ^{3}He), we ensure that the final state interaction with the spectator is small and the contributions from the current or target fragmentation of the hard process are suppressed. On the down side, the theoretical calculations are more difficult, however recent theoretical progress indicates that these calculations although tedious could be performed [34, 36, 37, 39, 43].

The quantity R^A which is defined by:

$$R^A(x_B, x'_B, Q^2, |\vec{P}_{A-1}|) \equiv \frac{\sigma_1^A(x_B, Q^2, |\vec{P}_{A-1}|, z_1^{(A)}, y_A)}{\sigma_1^A(x'_B, Q^2, |\vec{P}_{A-1}|, z_1^{(A)}, y_A)}, \tag{1.4}$$

represents the ratio between the cross sections on the nucleus A at two different values of the Bjorken scaling variable. Due to the cancellation of all the other terms but the nucleon structure functions in Eq. 1.4, R^A is highly sensitive to the nuclear effect. In the binding model (x-rescaling), where the inclusive nuclear structure function is expressed through a convolution of the nuclear spectral function and the structure function of the bound nucleon, one has

$$R^A(x_B, x'_B, Q^2, |\vec{P}_{A-1}|) = \frac{x'_B}{x_B} \frac{F_2^{N/A}(\frac{x_B}{z_1^A}, Q^2)}{F_2^{N/A}(\frac{x'_B}{z_1^A}, Q^2)}. \tag{1.5}$$

In the Q^2-rescaling model [18], which is based on the medium modification of the Q^2-evolution equations of QCD and the assumption that the quark confinement radius for a bound nucleon is larger than the one for a free nucleon, the ratio becomes

$$R^A(x_B, x'_B, Q^2, |\vec{P}_{A-1}|) = \frac{x'_B}{x_B} \frac{F_2^{N/A}(x_B, \xi_A(Q^2)Q^2)}{F_2^{N/A}(x'_B, \xi_A(Q^2)Q^2)} \tag{1.6}$$

While Eq. 1.5 is expected to depend both on A and $|\vec{P}_{A-1}|$, Eq. 1.6 would be a constant. By detecting nuclei with different recoil angles, this ratio would exhibit different behaviors, allowing a more detailed examination of the dynamics. Figure 1.4 shows theoretical predictions of the R^A ratio in the x- and Q^2-rescaling models at both perpendicular and backward recoil kinematics. We see there the power of discrimination of such measurement, between a model that link the EMC effect directly to the spectator momentum and one where it arises independently of it.

1.4 Tagged EMC ratio

Another observable used in theoretical calculations for the tagged EMC ratio is

$$R_0(x, Q^2) = \frac{\int_a^b \sigma_1^A d\vec{P}_{A-1}}{\int_a^b \sigma_1^D d\vec{P}_{A-1}}, \tag{1.7}$$

in which the cross section is integrated over a small momentum range of the recoil nucleus $\vec{P}_{A-1}$. In binding models it leads to opposite behavior for recoil nuclei emitted forward versus backward (Figure 1.5) that cancels in the usual inclusive EMC ratio. These resulting deviations are much larger than the usual inclusive EMC effect and provides opportunity for a significant experimental test of the binding models.
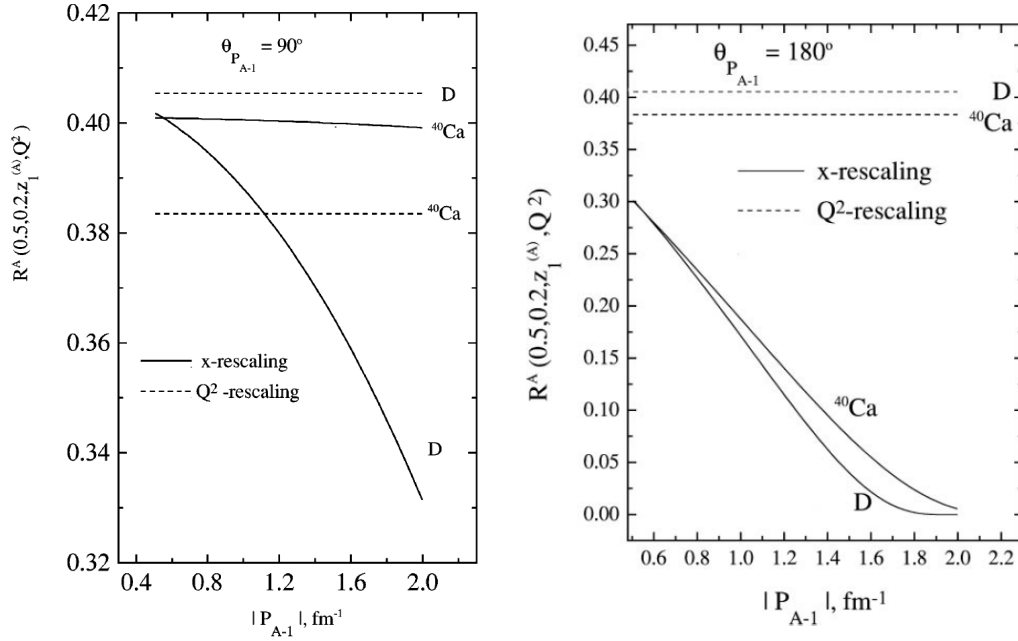
Figure 1.4: The ratio $R^A(x_B, x'_B)$ for $A = 2$ and $A = 40$, $x_B = 0.2$ and $x'_B = 0.5$, $Q^2 = 20$ GeV/c, plotted versus the momentum of the recoil nucleus $(A - 1)$ at perpendicular (left) and backward (right) angle $(\theta_{P_{A-1}} = 180°)$. The full and dashed curves are predictions of the x_B-rescaling (binding) and Q^2-rescaling models, respectively.

Figure 1.5: The semi-inclusive EMC ratio $R_0(x, Q^2)$ versus x with nuclei emitted forward and backward, the full curve is the usual inclusive EMC ratio, the dashed and dotted curves are predictions for the local EMC effect for different spectator recoil angles [23] (see the legend).

1.5 Flavor dependent parton distribution functions

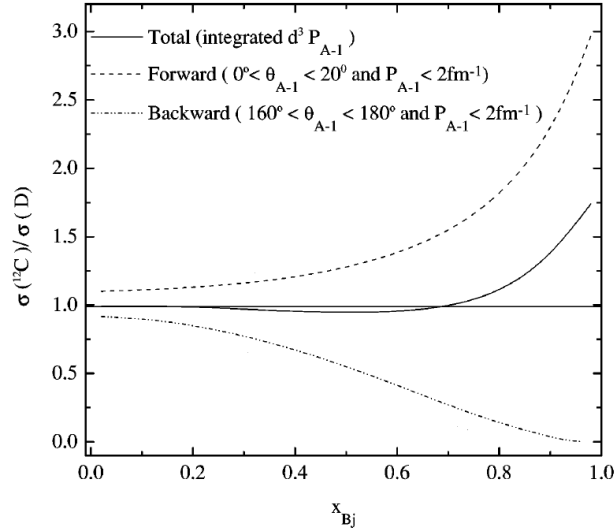Measurements of tagged structure functions have been carried out in CLAS by the e6 run group to study the EMC effect in deuteron [44] and later by the BONuS collaboration [47] to extract the F_2^n structure function by tagging the low momentum recoil proton. The main goal of the BONuS measurements was to extract the ratio F_2^n/F_2^p at high x_B and therefore access the ratio of down to up quark distribution (d/u) [32] at high x_B. By using ^{4}He targets and tagging the recoiling ^{3}He and ^{3}H nuclei, one can select scattering off a weakly or deeply bound neutron and proton respectively depending on their off-shellness in the ^{4}He nucleus. Since bound neutrons are always off-shell, even when $P_{^3He} = 0$, an extrapolation procedure is needed to extract the free (i.e. on-shell) neutron structure function from the tagged recoil data [48, 49]. One could measure the F_2 structure functions of a weakly bound neutron in ^{4}He and compare it to the ^{2}H data to detect any nuclear dependence. This procedure is necessary for neutrons due to the absence of a free neutron target. It can also be quantitatively benchmarked using the ^{4}He tagged data for scattering off a weakly bound proton, and comparing the results to the well measured free proton structure functions.

In addition, the ratio $(F_2^n/F_2^p)^{bound} / (F_2^n/F_2^p)^{free}$ can be measured to extract the distributions of d/u in a free nucleon and compare it to the same ratio for the bound nucleon. This is one way to explore the flavor dependent nuclear parton distributions which are little known experimentally. Such an effect, either in the anti-shadowing or EMC region, has been notably used to explain the NuTeV anomaly [50, 51].

1.6 Summary

In this chapter, we have shown very strong theoretical motivations to measure the tagged structure function of nucleons in light nuclei such as deuterium and helium. The main difficulty being to properly handle the FSI. To solve this challenge, a large acceptance detector is necessary in order to demonstrate that data match models on a wide kinematic range in angle and momentum. Moreover, such large acceptance detector needs also to work at the lowest possible energy to ensure that quasi-free nucleons of low off-shellness can be effectively compared with the more virtual ones. Our proposition for such a detector is presented in the next chapter.

We presented theoretical work suggesting that a measurement on deuterium will already show an effect, however we have also showed that higher nuclear masses provide much stronger signals and would ensure a compelling measurement. Observing several nuclei in different kinematics lead to very different results for the classic pure x_{Bj} and Q^2-rescaling models. This will allow us to determine precisely which picture or which combination of the two pictures is at the origin of the EMC effect. This measurement will therefore provide a completely new insight into the origin of the EMC effect and provide clear guidelines to build new models and better understand the partonic structure of nuclei.

In addition, our proposed experiment will allow to test the flavor symmetry of the nuclear effects, which have been discussed by theoretical predictions in the anti-shadowing and EMC regions. While this experiment is not dedicated to this question, for which additional isospin asymmetric targets would be necessary, we show that it can already provide a first test and pave the way for future works.

Chapter 2

Experimental Setup

All the different measurements of the ALERT run group require, in addition to a good scattered electron measurement, the detection of low energy nuclear recoil fragments with a large kinematic coverage. Such measurements have been performed in CLAS (BONuS and eg6 runs), where the adequacy of a small additional detector placed in the center of CLAS right around the target has shown to be the best solution. We propose here a similar setup using the CLAS12 spectrometer augmented by a low energy recoil detector.

We summarize in Table 2.1 the requirements for the different experiments proposed in the run group. By comparison with previous similar experiments, the proposed tagged measurements necessitate a good particle identification. Also, CLAS12 will be able to handle higher luminosity than CLAS so it will be key to exploit this feature in the future setting in order to keep our beam time request reasonable.

Measurement	Particles detected	p range	θ range
Nuclear GPDs	^{4}He	$230 < p < 400 MeV/c$	$\pi/4 < \theta < \pi/2$ rad
Tagged EMC	p, ^{3}H, ^{3}He	As low as possible	As close to π as possible
Tagged DVCS	p, ^{3}H, ^{3}He	As low as possible	As close to π as possible

Table 2.1: Requirements for the detection of low momentum spectator fragments of the proposed measurements.

This chapter will begin with a brief description of CLAS12. After presenting the existing options for recoil detection and recognize that they will not fulfill the needs laid out above, we will describe the design of the proposed new recoil detector ALERT. We will then present the reconstruction scheme of ALERT and show the first prototypes built by our technical
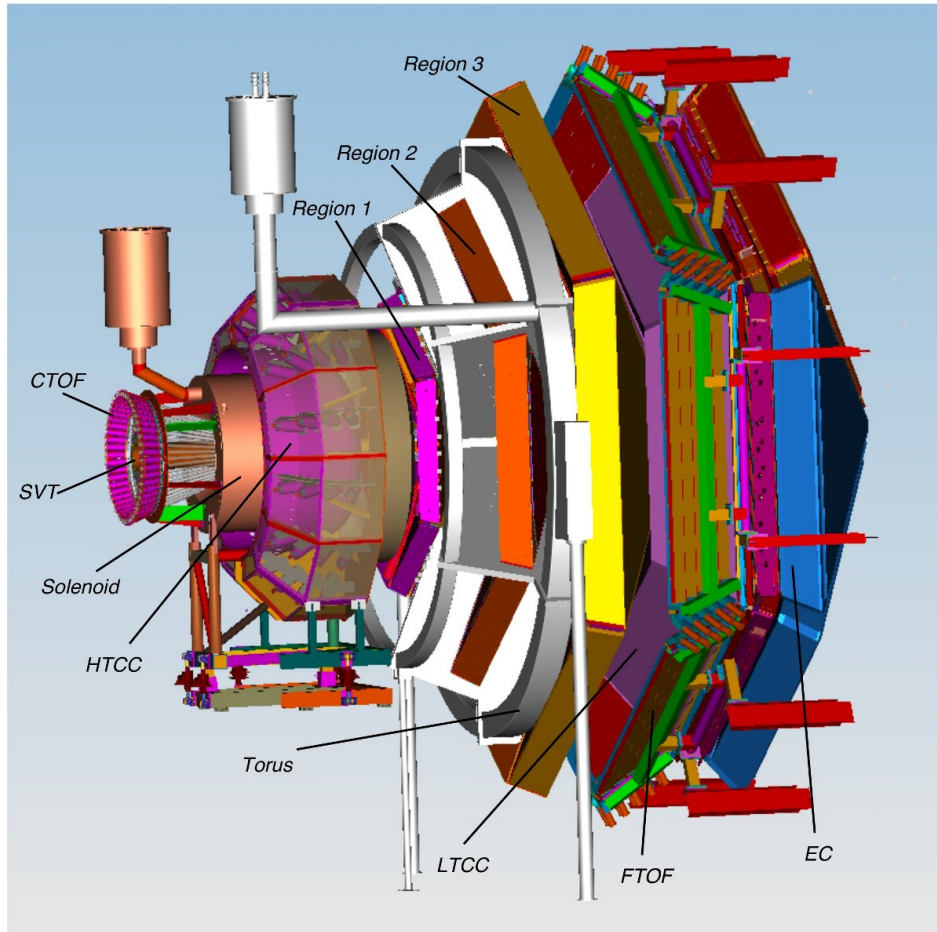
Figure 2.1: The schematic layout of the CLAS12 baseline design.

teams. Finally, we specify the technical contributions of the different partners.

2.1 The CLAS12 Spectrometer

The CLAS12 detector is designed to operate with 11 GeV beam at an electron-nucleon luminosity of $\mathcal{L} = 1 \times 10^{35}$ cm^{-2}s^{-1}. The baseline configuration of the CLAS12 detector consists of the forward detector and the central detector packages [52] (see Figure 2.1). We use the forward detector for electron detection in all ALERT run group proposals, while DVCS centered proposals also use it for photon detection. The central detector's silicon tracker and micromegas will be removed to leave room for the recoil detector.

The scattered electrons and photons will be detected in the forward detector which consists of the High Threshold Cherenkov Counters (HTCC), Drift Chambers (DC), the Low Threshold Cherenkov Counters (LTCC), the Time-of-Flight scintillators (TOF), the Forward Calorimeter and the Preshower Calorimeter. The charged particle identification in the forward detector is achieved by utilizing the combination of the HTCC, LTCC and TOF arrays with the tracking information from the Drift Chambers. The HTCC together with the Forward Calorimeter and the Preshower Calorimeter will provide a pion rejection factor of more than 2000 up to a momentum of 4.9 GeV/c, and a rejection factor of 100 above 4.9 GeV/c. The photons are detected using the calorimeters.

2.2 Available options for a Low Energy Recoil Detector

We explored available solutions for the low-energy recoil tracker with adequate momentum and spatial resolution, and good particle identification for recoiling light nuclei (p, ^{3}H and ^{3}He). After investigating the feasibility of the proposed measurements using the CLAS12 Central Detector and the BONuS Detector [47, 53], we concluded that we needed to build a dedicated detector. We summarize in the following the facts that led us to this conclusion.

2.2.1 CLAS12 Central Detector

The CLAS12 Central Detector [52] is designed to detect various charged particles over a wide momentum and angular range. The main detector package includes:

- Solenoid Magnet: provides a central longitudinal magnetic field up to 5 Tesla, which serves to curl emitted low energy Møller electrons and determine particle momenta through tracking in the central detector.

- Central Tracker: consists of 3 double layers of silicon strips and 6 layers of Micromegas. The thickness of a single silicon layer is 320 μm.

- Central Time-of-Flight: an array of scintillator paddles with a cylindrical geometry of radius 26 cm and length 50 cm; the thickness of the detector is 2 cm with designed timing resolution of $\sigma_t = 50$ ps, used to separate pions and protons up to 1.2 GeV/c.

The current design, however, is not optimal for low energy particles ($p < 300$ MeV/c) due to the energy loss in the first 2 silicon strip layers. The momentum detection threshold is ~ 200 MeV/c for protons, ~ 350 MeV/c for deuterons and even higher for ^{3}H and ^{3}He. These values are significantly too large for any of the ALERT run group proposals.

Detector Property	RTPC	ALERT
Detection region radius	4 cm	5 cm
Longitudinal length	~ 40 cm	~ 30 cm
Gas mixture	80% helium/20% DME	90% helium/10% isobutane
Azimuthal coverage	360°	340°
Momentum range	70-250 MeV/c protons	70-250 MeV/c protons
Transverse mom. resolution	10% for 100 MeV/c protons	10% for 100 MeV/c protons
z resolution	3 mm	3 mm
Solenoidal field	~ 5 T	~ 5 T
ID of all light nuclei	No	Yes
Luminosity	3×10^{33} nucleon/cm^2/s	6×10^{34} nucleon/cm^2/s
Trigger	can not be included	can be included

Table 2.2: Comparison between the RTPC (left column) and the new tracker (right column).

2.2.2 BONuS12 Radial Time Projection Chamber

The original BONuS detector was built for Hall B experiment E03-012 to study neutron structure at high x_B by scattering electrons off an almost on-shell neutron inside deuteron. The purpose of the detector was to tag the low energy recoil protons ($p > 60$ MeV/c). The key component for detecting the slow protons was the Radial Time Projection Chamber (RTPC) based on Gas Electron Multipliers (GEM). A later run period (eg6) used a newly built RTPC with a new design to detect recoiling α particles in coherent DVCS scattering. The major improvements of the eg6 RTPC were full cylindrical coverage and a higher data taking rate.

The approved 12 GeV BONuS (BONuS12) experiment is planning to use a similar device with some upgrades. The target gas cell length will be doubled, and the new RTPC will be longer as well, therefore doubling the luminosity and increasing the acceptance. Taking advantage of the larger bore (~ 700 mm) of the 5 Tesla solenoid magnet, the maximum radial drift length will be increased from the present 3 cm to 4 cm, improving the momentum resolution by 50% [53] and extending the momentum coverage. The main features of the proposed BONuS12 detector are summarized in Table 2.2.

In principle, particle identification can be obtained from the RTPC through the energy loss dE/dx in the detector as a function of the particle momentum (see Figure 2.2). However, with such a small difference between ^{3}H and ^{3}He, it is nearly impossible to discriminate between them on an event by event basis because of the intrinsic width of the dE/dx distributions.
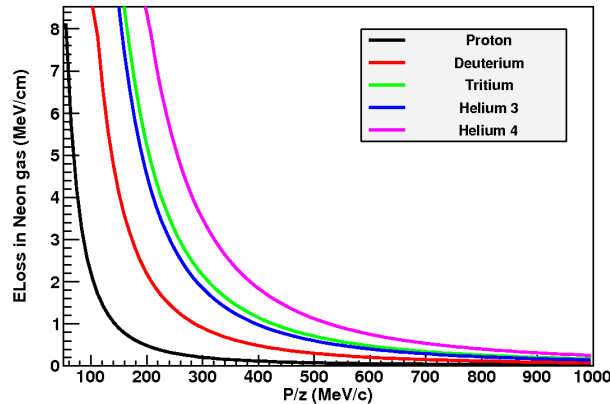
Figure 2.2: Calculation of energy loss in Neon gas as a function of the particle momentum divided by its charge for different nuclei.

This feature is not problematic when using deuterium target, but makes the RTPC no longer a viable option for our tagged EMC and tagged DVCS measurements which require a ^{4}He target and the differentiation of ^{4}He, ^{3}He, ^{3}H, deuterons and protons.

Another issue with the RTPC is its slow response time due to a long drift time (~ 5 μs). If a fast recoil detector could be included in the trigger it would have a significant impact on the background rejection. Indeed, in about 90% of DIS events on deuteron or helium, the spectator fragments have too low energy or too small angle to get out of the target and be detected. By including the recoil detector in the trigger, we would not be recording these events anymore. Since the data acquisition speed was the main limiting factor for both BONuS and eg6 runs in CLAS, this would be a much needed reduction of the pressure on the DAQ.

2.2.3 Summary

In summary, we found that the threshold of the CLAS12 inner tracker is significantly too high to be used for our measurements. On the other hand, the recoil detector planned for BONuS12, a RTPC, is not suitable due to its inability to distinguish all kind of particles we need to measure. Moreover, as the RTPC cannot be efficiently included in the trigger, a lot of background events are sent to the readout electronics, which will cause its saturation and limit the maximum luminosity the detector can handle. Therefore, we propose a new detector design.

2.3   Design of the ALERT Detector

We propose to build a low energy recoil detector consisting of two sub-systems: a drift chamber and a scintillator hodoscope. The drift chamber will be composed of 8 layers of sense wires to provide tracking information while the scintillators will provide particle identification through time-of-flight and energy measurements. To reduce the material budget, thus reducing the threshold to detect recoil particles at as low energy as possible, the scintillator hodoscope will be placed inside the gas chamber, just outside of the last layer of drift wires.

The drift chamber volume will be filled with a light gas mixture (90% He and 10% C_4H_{10}) at atmospheric pressure. The amplification potential will be kept low enough in order to not be sensitive to relativistic particles such as electrons and pions. Furthermore, a light gas mixture will increase the drift speed of the electrons from ionization. This will allow the chamber to withstand higher rates and experience lower hit occupancy. The fast signals from the chamber and the scintillators will be used in coincidence with electron trigger from CLAS12 to reduce the overall DAQ trigger rate and allow for operation at high luminosity.

The detector is designed to fit inside the central TOF of CLAS12; the silicon vertex tracker and the micromegas vertex tracker (MVT) will be removed. The available space has thus an outer radius of slightly more than 20 cm. A schematic layout of the preliminary design is shown in Figure 2.3 and its characteristics compared to the RTPC design in Table 2.2. The different detection elements are covering about 340° of the polar angle to leave room for mechanics, and are 30 cm long with an effort made to reduce the particle energy loss through the materials. From the inside out, it is composed of:

- a 30 cm long cylindrical target with an outer radius of 6 mm and target walls 25 µm Kapton filled with 3 atm of helium;

- a clear space filled with helium to reduce secondary scattering from the high rate Møller electrons with an outer radius of 30 mm;

- the drift chamber, its inner radius is 32 mm and its outer radius is 85 mm;

- two rings of plastic scintillators placed inside the gaseous chamber, with total thickness of roughly 20 mm.

2.3.1   The Drift Chamber

While drift chambers are very useful to cover large areas at a moderate price, huge progress has been made in terms of their ability to withstand higher rates using better electronics,
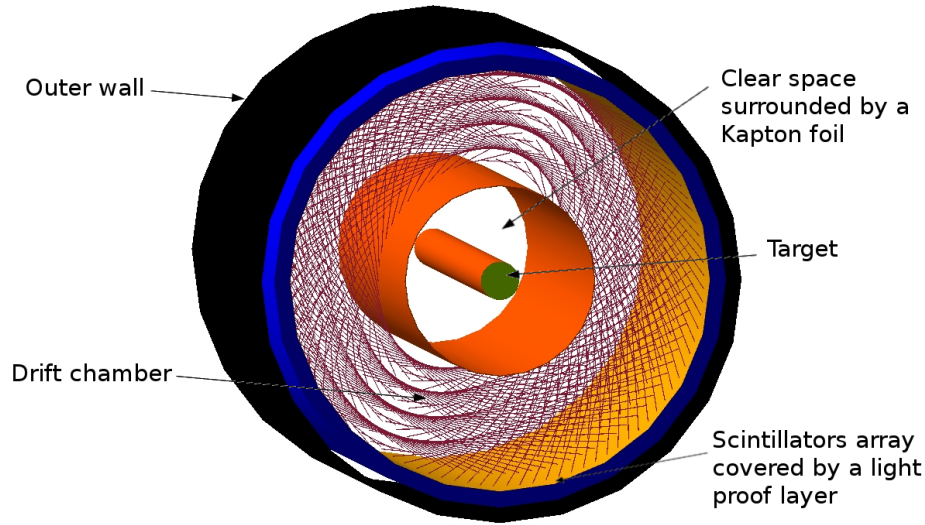
Figure 2.3: The schematic layout of the ALERT detector design, viewed from the beam direction.

shorter distance between wires and optimization of the electric field over pressure ratio. Our design is based on other chambers developed recently. For example for the dimuon arm of ALICE at CERN, drift chambers with cathode planes were built in Orsay [54]. The gap between sense wires is 2.1 mm and the distance between two cathode planes is also 2.1 mm, the wires are stretched over about 1 m. Belle II is building a cylindrical drift chamber very similar to what is needed for this experiment and for which the space between wires is around 2.5 mm [55]. Finally, a drift chamber with wire gaps of 1 mm is being built for the small wheel of ATLAS at CERN [56]. The cylindrical drift chamber proposed for our experiment is 300 mm long, and we therefore considered that a 2 mm gap between wires is technically a rather conservative goal. Optimization is envisioned based on experience with prototypes.

The radial form of the detector does not allow for 90 degrees x-y wires in the chamber. Thus, the wires of each layer are at alternating angle of $\pm$ 10°, called the stereo-angle, from the axis of the drift chamber. We use stereo-angles between wires to determine the coordinate along the beam axis (z). This setting makes it possible to use a thin forward end-plate to reduce multiple scattering of the outgoing high-energy electrons. A rough estimate of the tension due to the ∼2600 wires is under 600 kg, which appears to be reasonable for a composite end-plate.

The drift chamber cells are composed of one sense wire made of gold plated tungsten surrounded by field wires, however the presence of the 5 T magnetic field complicates the field lines. Several cell configurations have been studied with MAGBOLTZ [57], we decided
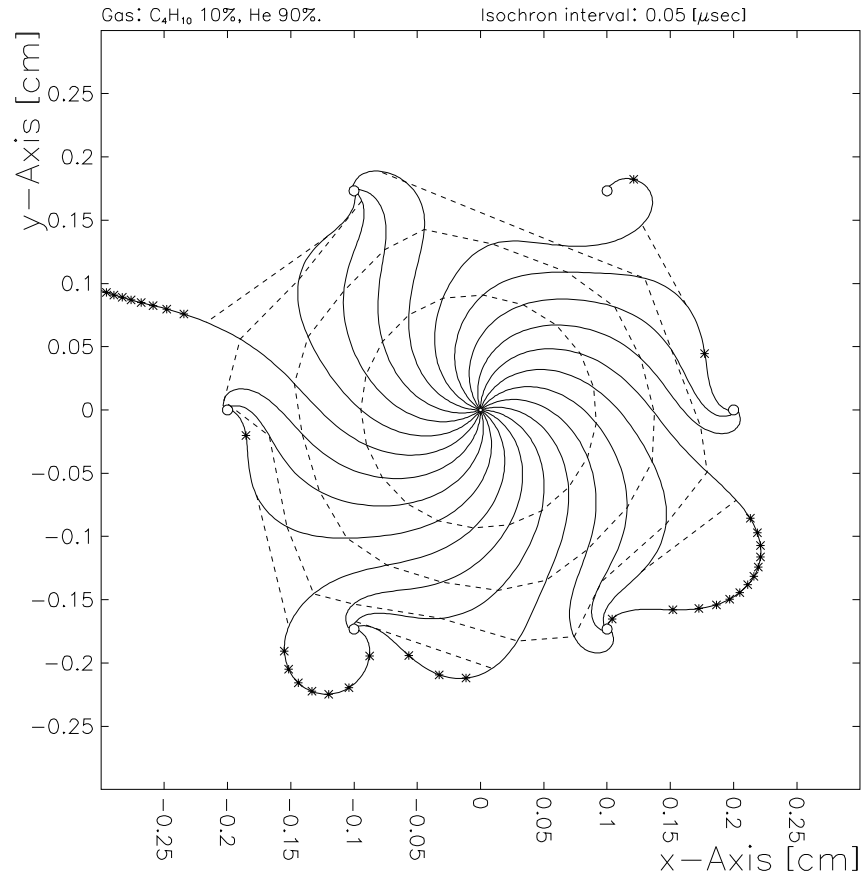
Figure 2.4: Drift lines simulated using MAGBOLTZ [57] for one sense wire (at the center) surrounded by 6 field wires. The two electric field lines leaving the cell disappear when adjusting the voltages on the wires. Dashed lines are isochrones spaced by 50 ns. This shows that the maximum drift time is about 250 ns.

to choose a conservative configuration as shown in Figure 2.4. The sense wire is surrounded by 6 field wires placed equidistantly from it in a hexagonal pattern. The distance between the sense and field wires is constant and equal to 2 mm. Two adjacent cells share the field wires placed between them. The current design will have 8 layers of cells of similar radius. The simulation code MAGBOLTZ is calculating the drift speed and drift paths of the electrons (Figure 2.4). With a moderate electric field, the drift speed is around 10 microns/ns, the average drift time expected is thus 250 ns (over 2 mm). Assuming a conservative 10 ns time resolution, the spatial resolution is expected to be around 200 microns due to field distortions and spread of the signal.

The maximum occupancy, shown in Figure 2.5, is expected to be around 5% for the inner most wires at 10^{35} cm^{-2}s^{-1} (including the target windows). This is the maximum
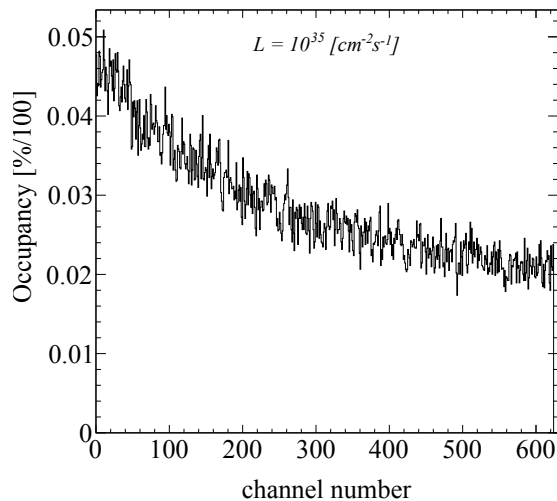
Figure 2.5: A full Geant4 simulation of the ALERT drift chamber hit occupancy at a luminosity of 10^{35} cm^{-2}s^{-1}. The channel numbering starts with the inner most wires and works outwards.

available luminosity for the baseline CLAS12 and is obtained based on the physics channels depicted in Figure 2.6, assuming an integration time of 200 ns and considering a readout wire separation of 4 mm. This amount of accidental hits does not appear to be reasonable for a good tracking quality, we therefore decided to run only at half this luminosity for our main production runs. This will keep occupancy below 3%, which is a reasonable amount for a drift chamber to maintain high tracking efficiency. When running the coherent processes with the ^{4}He target, it is not necessary to detect the protons[1], so the rate of accidental hits can then be highly reduced by increasing the detection threshold, thus making the chamber blind to the protons[2]. In this configuration, considering that our main contribution to occupancy are quasi-elastic protons, we are confident that the ALERT can work properly at 10^{35} cm^{-2}s^{-1}.

We are currently planning to use the electronics used by the MVT of CLAS12, known as the DREAM chip [58]. Its dynamic range and time resolution correspond to the needs of our drift chamber. To ensure that it is the case, tests with a prototype will be performed at the IPN Orsay (see section 2.5).

---

[1]This running condition is specific to the proposal "Partonic Structure of Light Nuclei" in the ALERT run group.

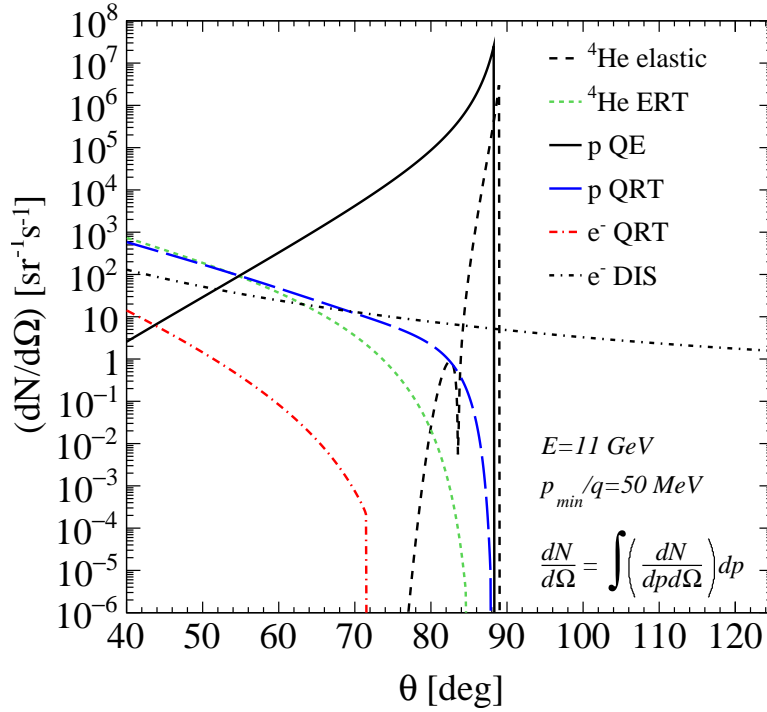[2]The CLAS *eg6* run period was using the RTPC in the same fashion.

Figure 2.6: The rates for different processes as function of angle. The quasi-elastic radiative tails (QRT), ^{4}He elastic radiative tail (ERT), and DIS contributions have been integrated over momenta starting at $p/q = 50$ MeV/c, where q is the electric charge of the particle detected.

2.3.2 The Scintillator Array

The scintillator array will serve two main purposes. First, it will provide a useful complementary trigger signal because of its very fast response time, which will reduce the random background triggers. Second, it will provide particle identification, primarily through a time-of-flight measurement, but also by a measurement of the particle total energy deposited and path length in the scintillator which is important for doubly charged ions.

The length of the scintillators cannot exceed roughly 40 cm to keep the time resolution below 150 ps. It must also be segmented to match with tracks reconstructed in the drift chamber. Since ^{3}He and ^{4}He will travel at most a few mm in the scintillator for the highest anticipated momenta ($\sim$ 400 MeV/c), a multi-layer scintillator design provides an extra handle on particle identification by checking if the range exceeded the thickness of the first scintillator layer.

The initial scintillator design consists of a thin (2 mm) inner layer of 60 bars, 30 cm in length, and 600 segmented outer scintillators (10 segments 3 cm long for each inner bar) wrapped around the drift chamber. Each of these thin inner bars has SiPM[3] detectors attached to both ends. A thicker outer layer (18 mm) will be further segmented along the beam axis to provide position information and maintain good time resolution.

For the outer layer, a dual ended bar design and a tile design with embedded wavelength shifting fiber readouts similar to the forward tagger's hodoscope for CLAS12 [59] were considered. After simulating these designs, it was found that the time resolution was insufficient except only for the smallest of tile designs ($15 \times 15 \times 7$ mm^3). Instead of using fibers, a SiPM will be mounted directly on the outer layer of a keystone shaped scintillator that is 30 mm in length and 18 mm thick. This design can be seen in Figure 2.7 which shows a full Geant4 simulation of the drift chamber and scintillators. By directly mounting the SiPMs to the scintillator we collect the maximum signal in the shortest amount of time. With the large number of photons we expect, the time resolution of SiPMs will be a few tens of ps, which is well within our target.

The advantage of a dual ended readout is that the time sum is proportional to the TOF plus a constant. The improved separation of different particles can be seen in Figure 2.8. Reconstructing the position of a hit along the length of a bar in the first layer is important for the doubly charged ions because they will not penetrate deep enough to reach the second layer of segmented scintillator.

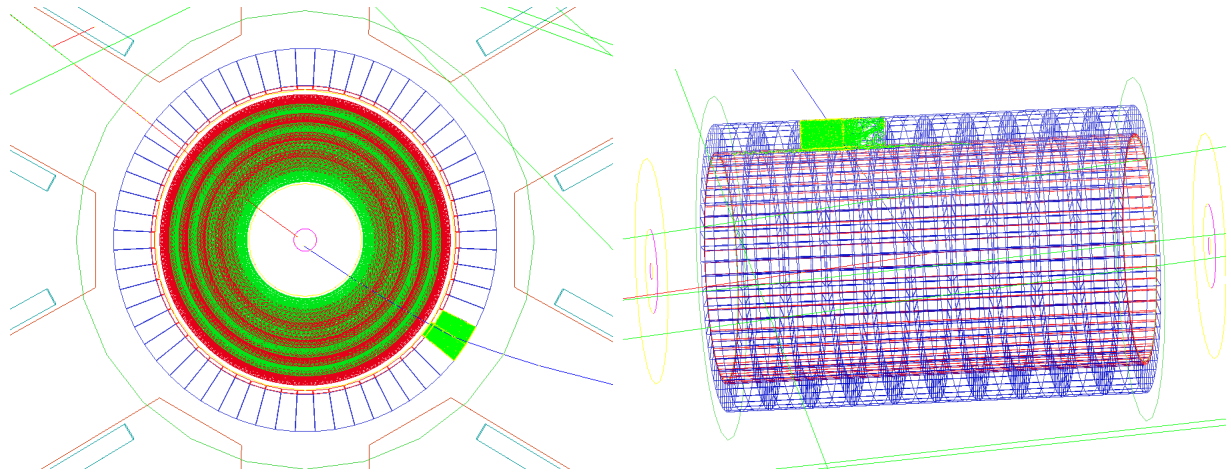---

[3]SiPM: silicon photomultiplier.

Figure 2.7: Geant4 simulation of a proton passing through the recoil drift chamber and scintillator hodoscope. The view looking downstream (left) shows the drift chamber's eight alternating layers of wires (green and red) surrounded by the two layers of scintillator (red and blue). Simulating a proton through the detector, photons (green) are produced in a few scintillators. On the right figure, the dark blue rings are graphical feature showing the contact between the adjacent outer scintillators.
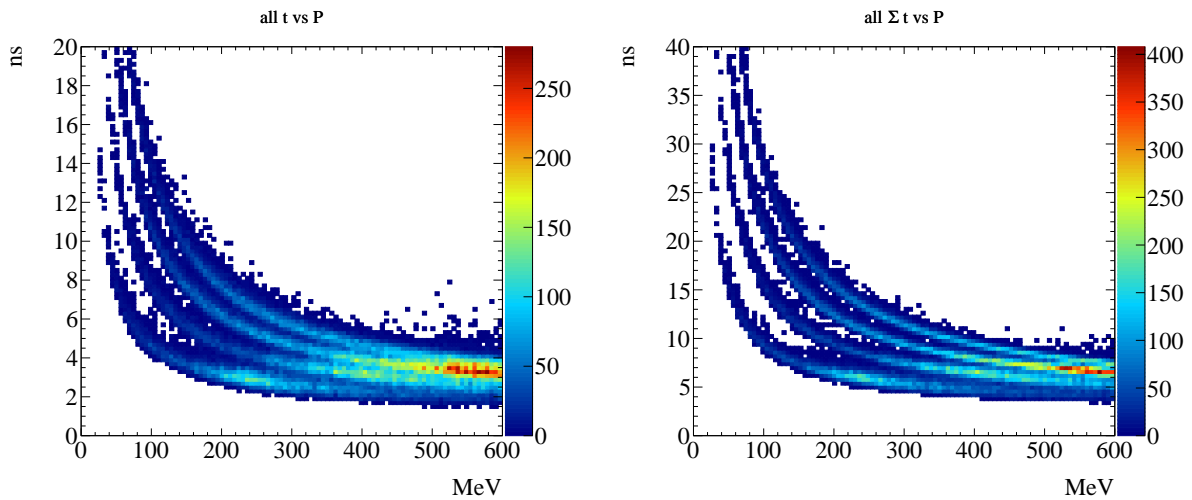

Figure 2.8: Simulated TOF for the various recoil particles vs Momentum. The TOF from just a single readout is shown on the left and the sum of the dual ended readout is shown on the right.

The front-end electrons for the SiPMs will include preamplifiers and ASICs[4] which provide both TDC and ADC readouts. The PETIROC-2A[60] ASIC provides excellent time resolution (18 ps on trigger output with 4 photoelectrons detected) and a maximum readout rate at about 40k events/s. Higher readout rates can be handled by using external digitizers by using the analog mode of operation and increase this rate by an order of magnitude. The ASIC also has the advantage of being able to tune the individual over-bias voltages with an 8-bit DAC.

The expected radiation damage to the SiPMs and scintillator material is found to be minimal over the length of the proposed experiment. We used the CLAS12 forward tagger hodoscope technical design report [59] as a very conservative baseline for this comparison. We arrived at an estimated dose of 1 krad after about 4.5 months of running. The damage to the scintillator at 100 times these radiation levels would not be problematic, even for the longest lengths of scintillator used [61]. Accumulated dose on the SiPMs leads to an increased dark current. Similarly than for scintillators, we do not expect it to be significant over the length of the experiment. The interested reader is referred to the work on SiPMs for the Hall-D detectors [62, 63]. A front-end electronics prototype will be tested for radiation hardness but we expect any damage to negligible [64].

2.3.3   Target Cell

The design of the proposed ALERT target will be very similar to the eg6 target shown in Figure 2.9. The target parameters are shown in Table 2.3 with the parameters of other existing and PAC approved targets. Note that, the proposed target has an increased radius of 6 mm compared to all the others which have 3 mm radius. This increase compared to the previous CLAS targets has been made in order to compensate for the expected increase of beam size at 11 GeV. The BONuS12 target is still presently proposed to be 3 mm in radius, if such a target is operated successfully in JLab, we will definitely consider using a smaller radius as well, but we prefer to propose here a safer option that we know will work fine.

2.4   Simulation of ALERT and reconstruction

The general detection and reconstruction scheme for ALERT is as follows. We fit the track with the drift chamber and scintillator position information to obtain the momentum over the charge. Next, using the scintillator time-of-flight, the particles are separated and identified by their mass-to-charge ratio, therefore leaving a degeneracy for the deuteron and
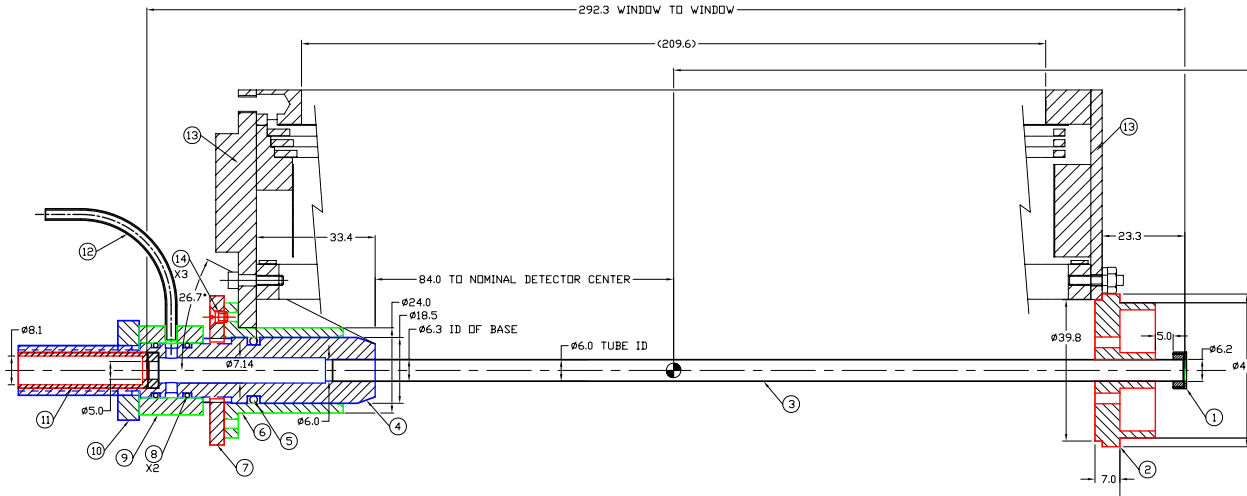
---

[4]ASIC: application-specific integrated circuit.

Figure 2.9: The eg6 target design drawing.

Table 2.3: Comparison of various straw targets used at JLab.The "JLab test targets" correspond to recent tests performed in JLab for the BONuS12 target, they have been tested for pressure but have never been tested with beam.

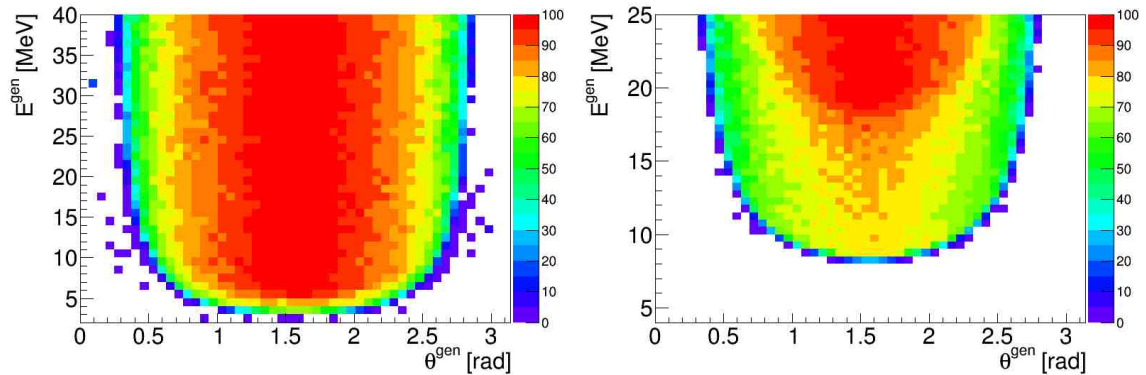| Experiment	Length	Kapton wall thickness	Pressure
CLAS target (eg6)	30 cm	$27\,\mu m$	6.0 atm
BONuS12 (E12-06-113) target	42 cm	$30\,\mu m$	7.5 atm
JLab test target 1	42 cm	$30\,\mu m$	3.0 atm
JLab test target 2	42 cm	$50\,\mu m$	4.5 atm
JLab test target 3	42 cm	$60\,\mu m$	6.0 atm
ALERT proposed target	35 cm	$25\,\mu m$	3.0 atm

Figure 2.10: Simulated recoil detector acceptance percentage, for protons (left) and ^{4}He (right), when requiring energy deposition in the scintillators arrays.

α particles. The degeneracy between deuteron and α particles can be resolved in a few ways. The first and most simple way is to observe that an α will almost never make it to the second layer of scintillators and therefore the absence (presence) of a signal would indicate the particle is an α (deuteron). Furthermore, as will be discussed below, the measured dE/dx will differ for ^{4}He and ^{2}H, therefore, taking into account energy loss in track fitting alone can provide separation. Additionally taking further advantage of the measured total energy deposited in the scintillators can help separate the αs and deuterons.

2.4.1 Simulation of ALERT

The simulation of the recoil detector has been implemented with the full geometry and material specifications in GEANT4. It includes a 5 Tesla homogeneous solenoid field and the entire detector filled with materials as described in the previous section. In this study all recoil species are generated with the same distributions: flat in momentum from threshold up to 40 MeV ($\sim$ 250 MeV/c) for protons and about 25 MeV for other particles; isotropic angular coverage; flat distribution in z-vertex; and a radial vertex coordinate smeared around the beam line center by a Gaussian distribution of sigma equal to the expected beam radius (0.2 mm). For reconstruction, we require that the particle reaches the scintillator and obtain the acceptance averaged over the z-vertex position shown in Figure 2.10.
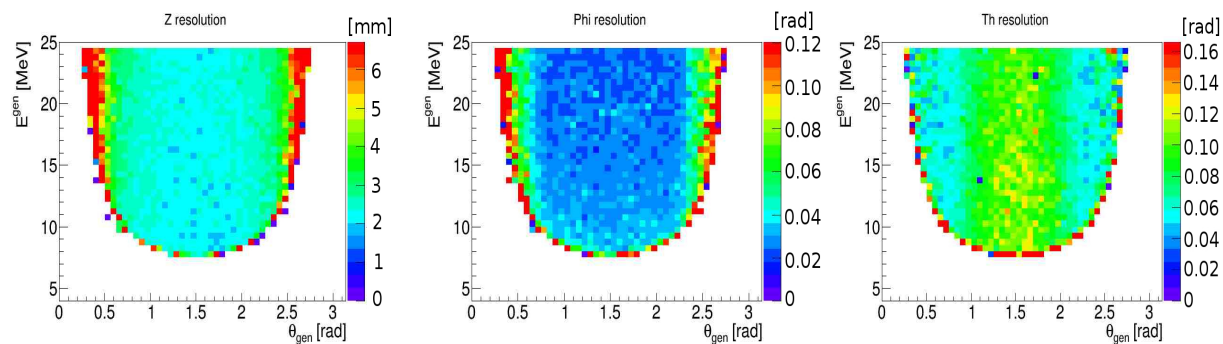
Figure 2.11: Resolutions for simulated ^{4}He: z-vertex resolution in mm (left), azimuthal (center) and polar (right) angle resolutions in radians for the lowest energy regime when the recoil track reaches the scintillator.

2.4.2   Track Fitting

The tracks are obtained using a helix fitter giving the coordinates of the vertex and the momentum of the particle. The energy deposited in the scintillators could also be used to help determine the kinetic energy of the nucleus, but is not implemented in the studies we performed here. The tracking capabilities of the recoil detector are investigated assuming a spatial resolutions of 200 µm for the drift chamber. The wires are strung in the z-direction with a stereo angle of 10°. The resulting difference between generated and reconstructed variables from simulation is shown in Figure 2.11 for ^{4}He particles. The momentum resolution for both protons and ^{4}He is presented in Figure 2.12.

2.4.3   Particle identification in ALERT

The particle identification scheme is investigated using the GEANT4 simulation as well. The scintillators have been designed to ensure a 150 ps time resolution. To determine the dE/dx resolution, measurements will be necessary for the scintillators and for the drift chamber as this depends on the detector layout, gas mixture, electronics, voltages... Nevertheless, from [65], one can assume that with 8 hits in the drift chamber and the measurements in the scintillators, the energy resolution should be at least 10%. Under these conditions, a clean separation of three of the five nuclei is shown in Figure 2.13 solely based on the time of flight measured by the scintillator compared to the reconstructed momentum from the drift chamber. We then separate ^{2}H and α using dE/dx in the drift chamber and in the scintillators.

To quantify the separation power of our device, we simulated an equal quantity of each
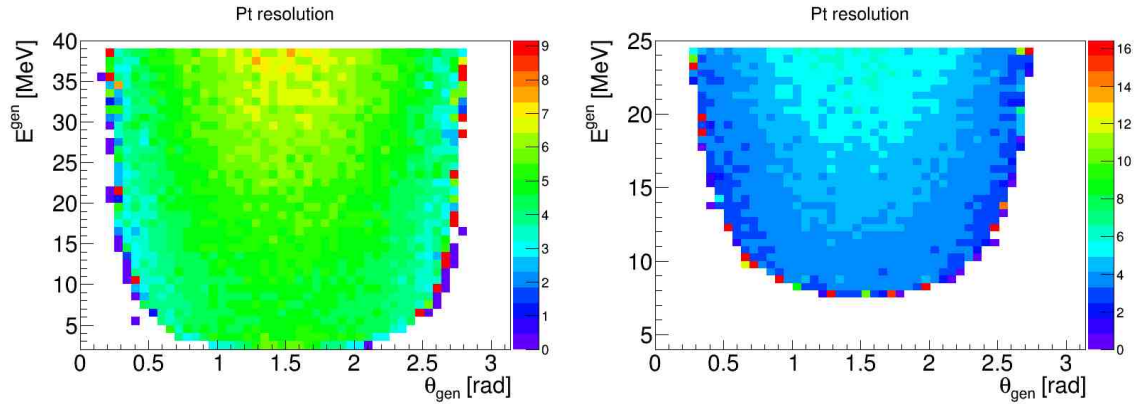
Figure 2.12: Simulated momentum resolutions (in %) as a function of energy and polar angle for protons (left) and ^{4}He (right) integrated over all z, when the recoil track reaches the scintillators array.
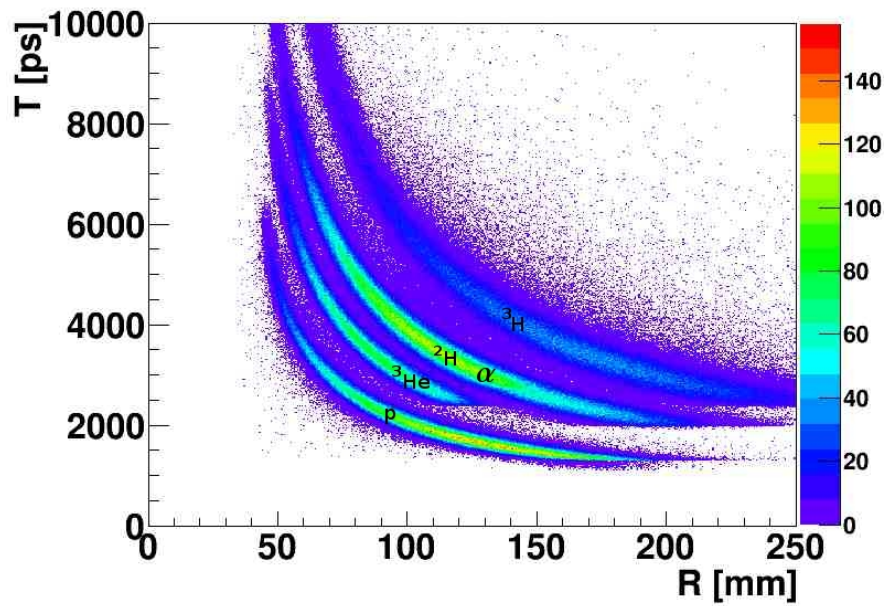
Figure 2.13: Simulated time of flight at the scintillator versus the reconstructed radius in the drift chamber. The bottom band corresponds to the proton, next band is the ^{3}He nuclei, ^{2}H and α are overlapping in the third band, the uppermost band is ^{3}H. ^{2}H and α are separated using dE/dx.

species. We obtained a particle identification efficiency of 99% for protons, 95% for ^{3}He and 98% for ^{3}H and around 90% for ^{2}H and α with equally excellent rejection factors. It is important to note that for this analysis, only the energy deposited in the scintillators was used, not the energy deposited in the drift chamber nor the path length in the scintillators, thus these numbers are very likely to be improved when using the full information[5]. This analysis indicates that the proposed reconstruction and particle identification schemes for this design are quite promising. Studies, using both simulation software and prototyping, are ongoing to determine the optimal detector parameters to minimize the detection threshold while maximizing particle identification efficiency. The resolutions presented above have been implemented in a fast Monte-Carlo used to evaluate their impact on our measurements.

2.5 Drift chamber prototype

Since the design of the drift chamber presents several challenges in term of mechanical assembly, we decided to start prototyping early. The goal is to find a design that will be easy to install and to maintain if need be, while keeping the amount of material at a minimum. This section presents the work done in Orsay to address the main questions concerning the mechanics that needed to be answered:

- How to build a stereo drift chamber with a 2 mm gap between wires?

- Can we have frames that can be quickly changed in case of a broken wire?

- How to minimize the forward structure to reduce the multiple scattering, while keeping it rigid enough to support the tension due to the wires?

For the first question, small plastic structures realized with a 3D printer were tested and wires welded on it, as shown in Figure 2.14. This demonstrated our ability to weld wires with a 2 mm gap on a curved structure.

To limit issues related to broken wires, we opted for a modular detector made of identical sectors. Each sector covers 20° of the azimuthal angle (Figure 2.15) and can be rotated around the beam axis to be separated from the other sectors. This rotation is possible due to the absence of one sector, leaving a 20° dead angle. Then, if a wire breaks, its sector can be removed independently and replaced by a spare. Plastic and metallic prototype sectors were made with 3D printers to test the assembling procedure and we have started the construction

---

[5]The uncertainty remains important about the resolutions that will be achieved for these extra information. So we deemed more reasonable to ignore them for now.
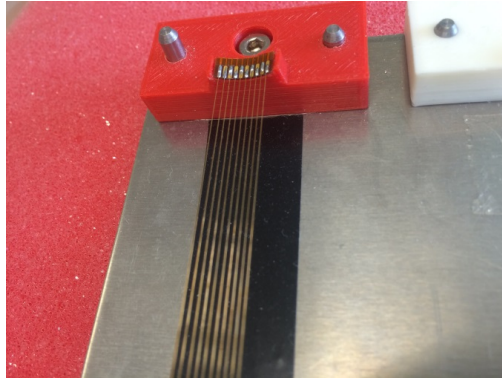
Figure 2.14: Welded wires on a curved structure with a 2 mm gap between each wire.
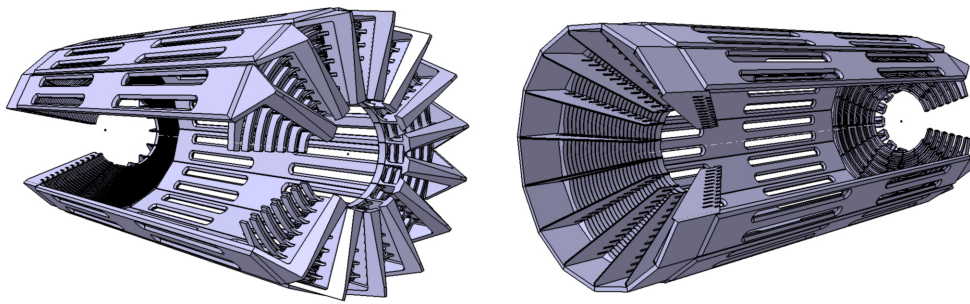
Figure 2.15: Upstream (left) and downstream (right) ends of the prototype detector in computer assisted design (CAD) with all the sectors included.

of a full size prototype of one sector. The shape of each sector is constrained by the position of the wires. It has a triangular shape on one side and due to the stereo angle, the other side looks like a pine tree with branches alternatively going left and right from a central trunk (Figure 2.16).

Finally, the material used to build the structure will be studied in details with future prototypes. Nevertheless, most recent plans are to use high rigidity plastic in the forward region and metal for the backward structure (as in Figure 2.17). The prototypes are not only designed to check the mechanical requirements summarized above but also to verify the different cell configurations, and to test the DREAM electronics (time resolution, active range, noise).

Figure 2.16: Close up on the CAD of the upstream piece (left) and downstream piece(right) of the drift chamber. Note that the design of the pieces has been optimized in comparison of what is shown in Figure 2.15.
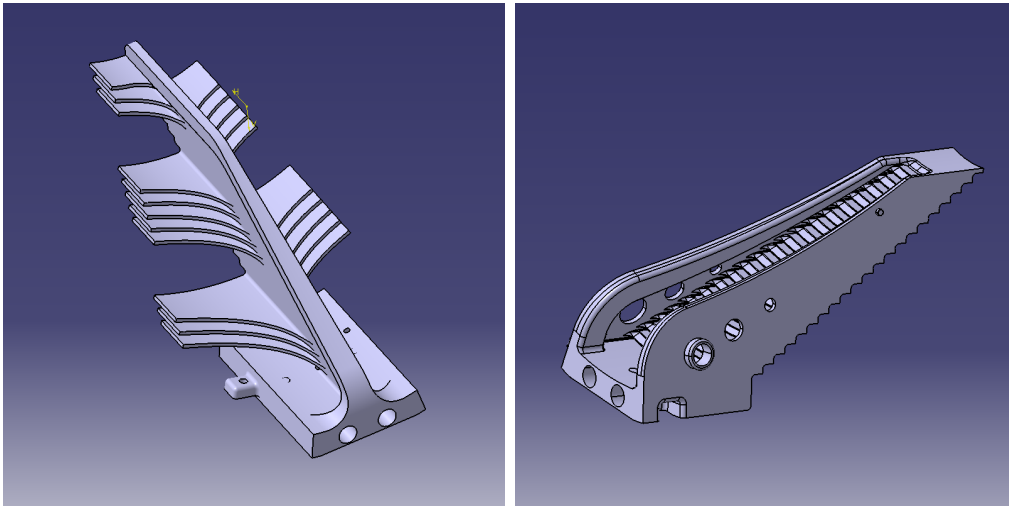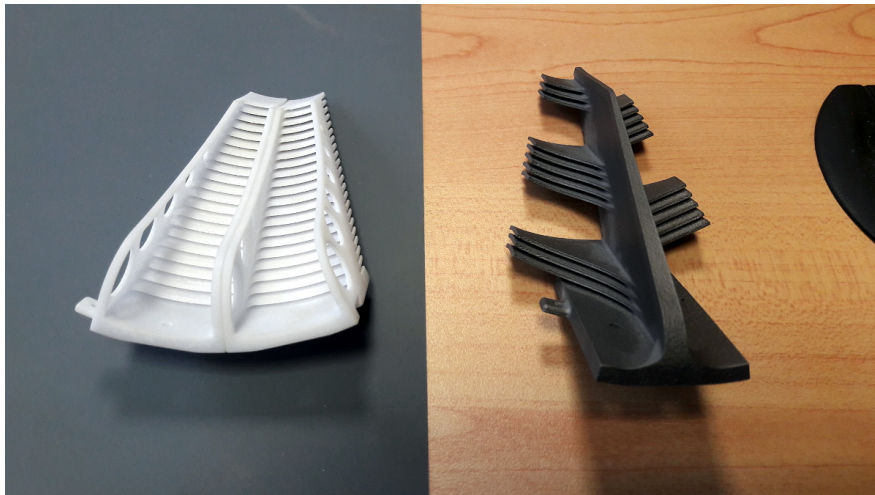

Figure 2.17: Prototypes for the mechanical parts of the drift chamber made out of plastic for the forward part and titanium for the backward.

2.6   Technical contributions from the research groups

The effort to design, build and integrate the ALERT detector is led by four research groups, Argonne National Lab (ANL), Institut de Physique Nucléaire d'Orsay (IPNO), Jefferson Lab and Temple University (TU).

Jefferson Lab is the host institution. ANL, IPNO and TU have all contributed technically to CLAS12. ANL was involved in the construction of the high-threshold Cherenkov counters (HTCC) for CLAS12. ANL has a memorandum of understanding (MOU) with JLab on taking responsibility for the HTCC light collection system including testing the photomultipliers and the magnetic shielding. For the RICH detector for CLAS12, ANL developed full GEANT-4 simulations in addition to the tracking software. ANL also developed the mechanical design of the detector support elements and entrance and exit windows in addition to the front-end electronics cooling system. IPNO took full responsibility for the design and construction of CLAS12 neutron detector (CND). The CND was successfully delivered to Jefferson Lab. TU played an important role in the refurbishment of the low threshold Cherenkov counters (LTCC), which was completed recently. All 216 photomultipliers have been coated with wavelength shifting material (p-Terphenyl) at Temple University, which resulted in a significant increase in the number of photoelectrons response.

The three institutions have already shown strong technical commitment to JLab 12 GeV upgrade, with a focus on CLAS12 and this proposal is a continuation of this commitment.

2.6.1   Argonne National Laboratory and Temple University

The ANL medium energy group is responsible for the ALERT scintillator system, including scintillation material, light collection device and electronics. First results of simulations have led to the design proposed here. This work will continue to integrate the scintillator system with the wire chamber. ANL will collaborate closely with Temple University to test the light detection system. Both institutions will be responsible to assemble and test the detector.

Argonne will provide the electronics and technical support required to integrate the scintillator detector system into the CLAS12 DAQ. The effort will minimize the effort required on the part of the Hall B staff.

2.6.2   Institut de Physique Nucléaire d'Orsay

The Institut de Physique Nucléaire d'Orsay is responsible for the wire chamber and the mechanical structure of the detector design and construction. As shown in the proposal, this work has already started, a first prototype is being built to test different cell forms, wire material, wire thickness, pressure, etc. This experience will lead to a complete design of the ALERT detector integrating the scintillator built at ANL, the gas distribution system and the electronic connections.

In partnership with *CEA Saclay*, IPN Orsay will also test the use of the DREAM front-end chip for the wire chamber. Preliminary tests were successful and will continue. The integration of the chip with CLAS12 is expected to be done by the *CEA Saclay*, since they use the same chip to readout the CLAS12 MVT. Adaptations to the DAQ necessary when the MVT will be replaced by ALERT will be performed by the staff of IPN Orsay.

2.6.3   Jefferson Laboratory

We expect Jefferson Lab to help with the configuration of the beam line. This will include the following items.

Beam Dump Upgrade   The maximum beam current will be around 1000 nA for the production runs at 10^{35} cm^{-2}s^{-1}, which is not common for Hall-B. To run above 500 nA the "beam blocker" will need to be upgraded to handle higher power. The beam blocker attenuates the beam seen by the Faraday cup. This blocker is constructed of copper and is water cooled. Hall B staff have indicated that this is a rather straightforward engineering task and has no significant associated costs [66].

Straw Target   We also expect JLab to design and build the target for the experiment as it will be a very similar target as the ones build for CLAS BONuS and eg6 runs. See section 2.3.3 for more details.

Mechanical Integration   We also expect Jefferson Laboratory to provide assistance in the detector installation in the Hall. This will include providing designers at ANL and IPNO with the technical drawings required to integrate ALERT with CLAS12. We will also need some coordination between designers to validate the mechanical integration.

CLAS12 DAQ Integration We also will need assistance in connecting the electronics of ALERT to the CLAS12 data acquisition and trigger systems. This will also include help integrating the slow controls into the EPICs system.

Chapter 3

Proposed Measurements

In light of the physics motivation presented and the capabilities of the new ALERT detector, we propose to measure the tagged deep-inelastic scattering off ^{2}H and ^{4}He and for a range of the recoiling spectator momenta P_{A-1} from 70 to 400 MeV/c. We choose the helium target for several reasons, first it is a light gas that can easily be used in a very light gaseous target allowing to detect very low momentum spectators. Also, calculation for FSI are theoretically very challenging, keeping the number of nucleon low is therefore of great help; moreover, as spectators get heavier, their detection threshold increases, which explains why we want to use low A target. The reactions we are going to study are:

- ^{2}H$(e, e'p)X$ — bound neutron;

- ^{4}He$(e, e'\ ^3$H$)X$ — bound proton;

- ^{4}He$(e, e'\ ^3$He$)X$ — bound neutron;

3.0.1 Monte-Carlo Simulation

To estimate the rates of our experiment and provide meaningful estimates of our statistical error bars, we developed a Monte-Carlo simulation based on PYTHIA to which we added nuclear Fermi motion effects. The interaction on the nucleon is generated in a basic impulse approximation, neglecting the off-shellness of the target nucleon. We simulate the Fermi motion of the nucleons in the target nuclei according to the distribution provided by AV18+UIX potentials [67, 68, 69]. This leads to a target nucleon with momentum $\vec{p}_n$ and a nuclear spectator generated with a kinematic opposite to the interacting nucleon, $-\vec{p}_n$. The

PYTHIA Monte-Carlo provides simulation for the DIS interaction and the fragmentation of the partons, we do not include nuclear effects such as FSI here. This should not be an issue for our estimate as our key measurements are focused on the parts of the phase space where the FSI are small.

In the simulation, we select DIS by requesting $Q^2 > 1.5$ GeV^2 and $W > 2$ GeV. These are the same for all figures, indication on the figures are for the theoretical predictions. In our experimental configuration and with the cut described above, we expect $\langle Q^2 \rangle \sim 3$ GeV^2.

The generated final-state particles undergo acceptance tests. Electrons, which will be detected by the forward detector, are treated by a GEANT4 Monte-Carlo simulation of CLAS12. The recoiling nuclei (including protons) acceptance is based on the GEANT4 simulation described in section 2.4 and represented in Figure 2.10. On top of these estimates, we apply an overall 75% efficiency to this detection settings to account for the fiducial cuts and detector inefficiencies.

3.0.2 Beam Time Request

We estimate, based on past measurements with CLAS [70], that the ratios we want to measure will be affected by systematic errors of ~ 3 percents. The dominant factor being associated to acceptance corrections. Our beam time request, allows to have the statistical error bars of our key measurement (Figure 3.4 right) comparable to the systematic ones. Assuming the luminosity of 3.10^{34} cm^{-2}s^{-1}, the beam time request for proposed measurements is of 20 days for each target.

3.1 Projections

Based on our simulation, we determine the available kinematic range and production rates accessible for each channel. The x_B and recoil momenta distributions are illustrated in Figure 3.1 for tagged ^3H out of an ^{4}He target. This figure shows the available phase space for a measurement of the bound proton structure function.
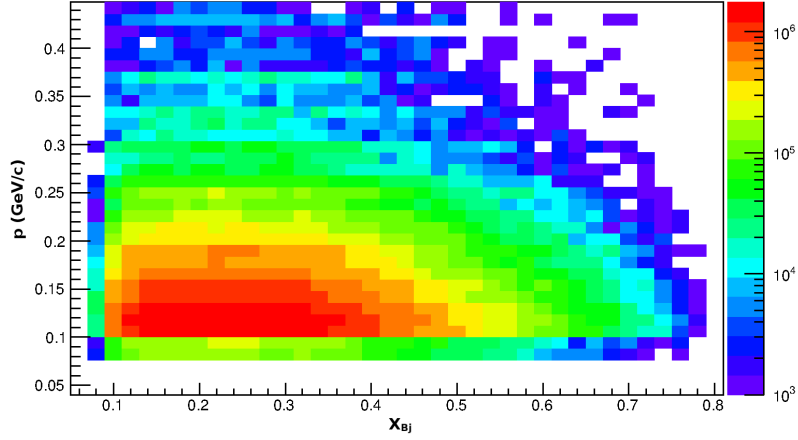
Figure 3.1: Expected event count as a function of x_B and the recoil momentum of the ^{3}H from a ^{4}He target.
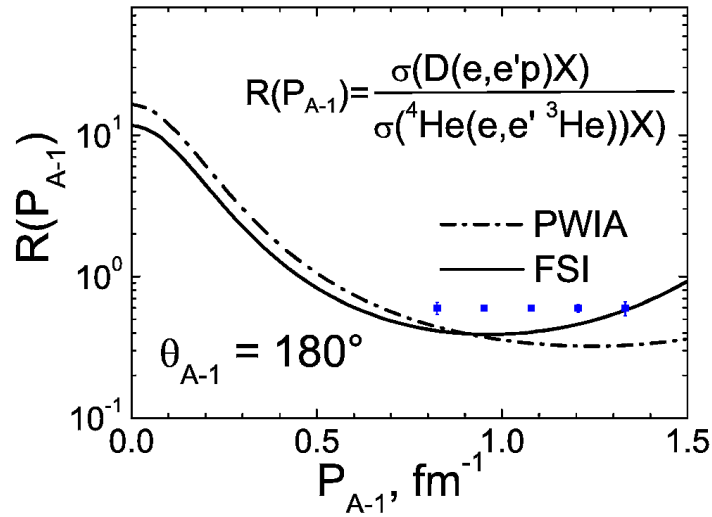

Figure 3.2: This figure is similar to Figure 1.2, it shows the predictions for the ratio $R(A, A', |\vec{P}_{A-1}|)$ for CLAS12 kinematic [23, 71] compared to our projected statistical error bars (blue points).

3.1.1 Testing the Spectator Model

The projections presented in Figure 3.2 show the capability of this experiment to measure cross section ratios of DIS on a bound nucleon in light nuclei and, therefore, our capability to check the validity of the spectator model used by the theoretical predictions. Statistical error bars in this figure are very modest and even smaller than the points on the logarithmic scale. It is therefore clear that we have capability to test the spectator model in more details with multi-dimensional binning as was done in [72] and for the first time perform similar studies on helium. However, we do not have specific model predictions for such measurement to compare with at the moment.

Other tests have been proposed to insure that outgoing pions are formed far enough from the nuclei to limit FSI [73, 74] and understand the color transparency effect associated. This study is most sensitive to spectators emitted at 90°, where the effect is larger, and can then be extrapolated to lower angles. In Ref. [49], testing that the x_B scaling holds in tagged DIS is proposed as another way to confirm the soundness of the method.

As shown above, the high statistics of the experiment will open the possibility to make several tests of the spectator mechanism and its limits. In particular it will, for the first time, experimentally explore this question for helium, opening the way for light nuclei tagged experiments.

3.1.2 EMC effect in deuterium

As explained in the first chapter, it is possible to enhance the EMC effect in the deuteron by selecting the highly off-shell nucleons. This prediction can be directly tested with our proposed experiment, as shown in Figure 3.3 where we compare our measurement capabilities to Melnitchouk *et al.* [40] predictions for rescaling models as well as the PLC suppression model. Note than in our case, the proton being tagged, we are actually measuring F_{2n}^{bound}/F_{2n}, but this measurement can be interpreted similarly to the proton case in regard to the EMC effect. The main limitation in this channel is the very fast decrease of the cross section for high α in deuterium.

We point out that such a measurement is also possible with the helium target, for either the proton or the neutron. This would allow to reach much higher *alpha* without running a prohibitively long experiment. We do not present these projections here because, at the moment, there is no theoretical predictions for these channels. The main reason is the difficulty to extend the calculations to the helium four-body system. However, we have
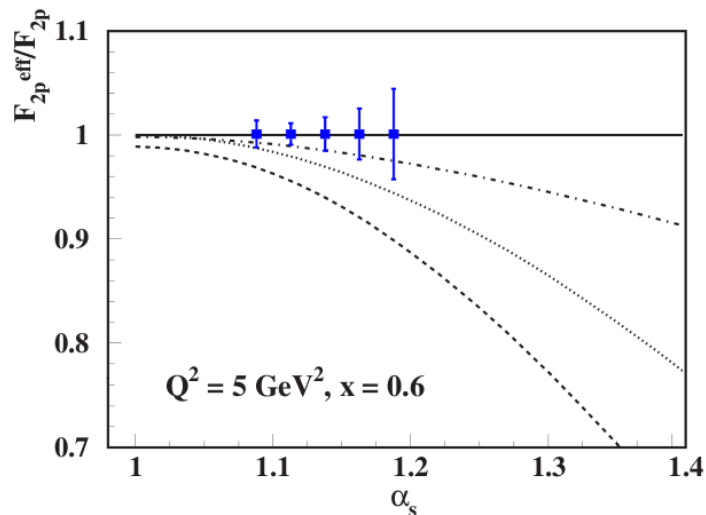
Figure 3.3: This figure is similar to Figure 1.3, it shows the predictions from [40] of the ratio F_{2p}^{bound}/F_{2p} compared to projected statistical error bars for the proposed experiment (blue points). Dashed line is a prediction for the PLC suppression model, dotted is for the Q^2-rescaling model, and dot-dashed for the binding/off-shell model.

indications that these kind of studies are on-going in the theory community [75].

3.1.3 Testing the Rescaling Models

The main goal of our experiment is to discriminate decisively between models of EMC, Figure 3.4 illustrates this capability. We have here a high differentiation power between x-rescaling and Q^2-rescaling models. We note the good coverage and small error bars for $\theta_{P_{A-1}} = 90°$ ($75 < \theta_{P_{A-1}} < 105°$). This is due to the better acceptance for this angle. The measurement at backward angle ($\theta_{P_{A-1}} > 150°$), however, is much more difficult and is the main constraint driving our beam time request. Still, in order to obtain our planned precision with a reasonable beam time request, the backward angles are selected from 150° and up instead of the 160° which is used for the theory predictions.

We notice the complementarity of our choice of targets in the phase space covered, this is due to the fact that larger recoil nuclei are more absorbed by the target material and have higher detection threshold. At the same time, the Fermi momentum is larger in helium allowing better statistics at high p_{A-1}. Using helium is then also an opportunity to explore higher spectator momentum with a reasonable beam time request.
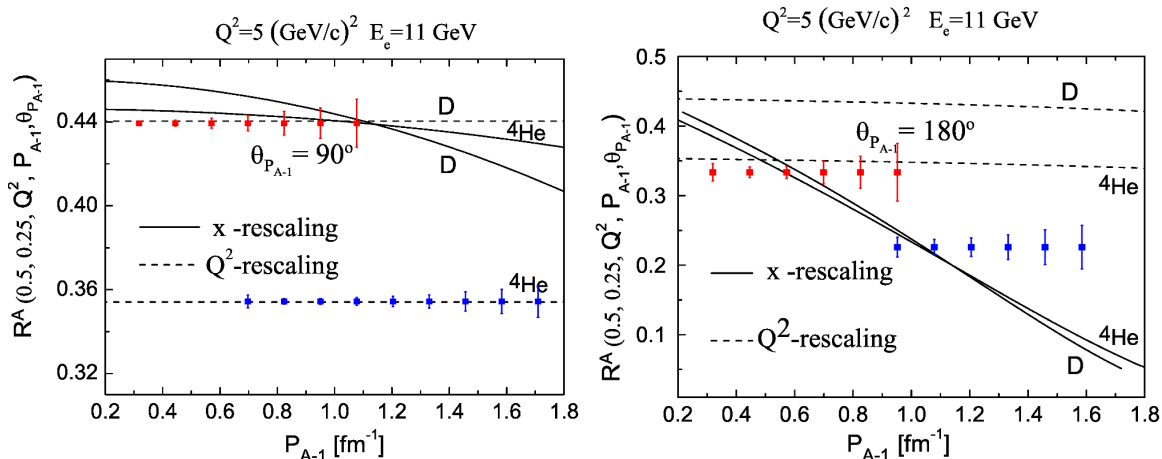
Figure 3.4: This figure is similar to figure 1.4, it shows predictions of the ratio $R^A(x, x')$ for $A = 2$ and $A = 4$ as a function of the momentum of the recoil nucleus $A - 1$ at perpendicular (left) and backward (right) angle. The full and dashed curves are predictions for CLAS12 kinematic [23, 71] of the x-rescaling (binding) and Q^2-rescaling models, respectively, points are projections for ^2H (red) and ^4He (blue).

3.1.4 Tagged EMC Ratio

The experiment can also confront the striking predictions for backward versus forward tagged EMC in binding models, as illustrated in the Figure 3.5. We see that the model prediction will be clearly tested, however the reach in x_B for the backward recoils is also strongly constrain by the beam time available for the experiment. Indeed, the strongest effect is expected at $x_B \sim 0.5$ for which we need high statistics.

The measurement of the tagged EMC ratio is a very good observable even for other kinds of model, in the low momentum regime one should be able to reproduce very nicely the classic EMC effect and then be able to study its dependence to the spectator angle and momentum. In general, models based only on off-shellness predict no differences between nuclei at a given spectator kinematic. This prediction can be tested nicely with the measurement presented here.
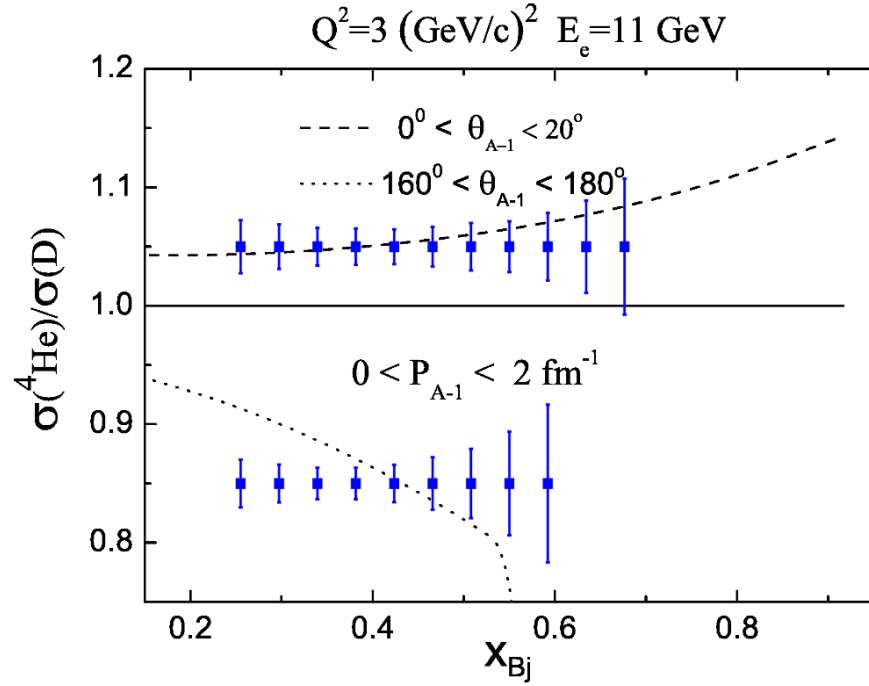
Figure 3.5: This figure is similar to figure 1.5, it shows the semi-inclusive EMC ratio $R_0(x, Q^2)$ as a function of x_B with recoils emitted forward and backward, the dashed and dotted curves are predictions for the local EMC effect for CLAS12 kinematic [23, 71] the blue points are statistical error bar projections for our measurement.
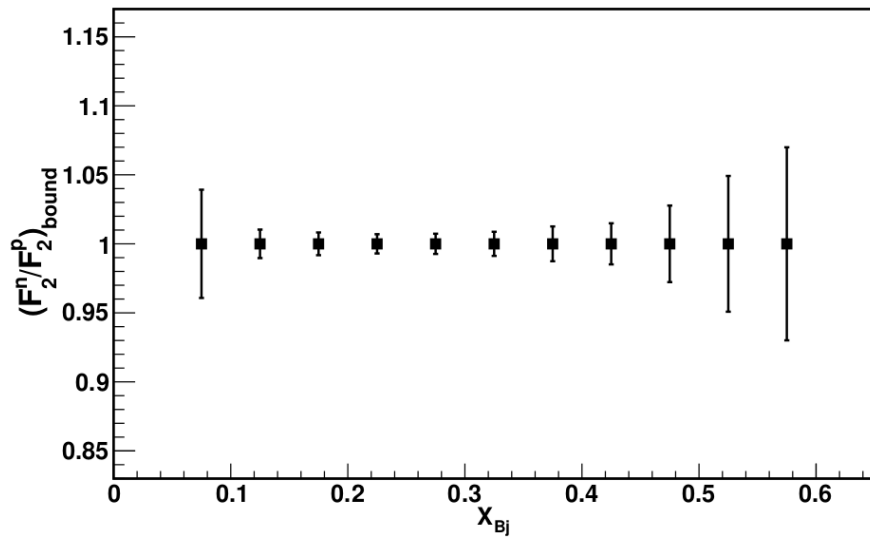
Figure 3.6: Statistical error bar projections for the ratio F_2^n/F_2^p for bound nucleons as a function of x_{Bj} using an ^{4}He target.

3.1.5 The Flavor Dependent Nuclear Effects

Finally with our experimental setup, we will explore the flavor dependence of nuclear PDFs. Figure 3.6 illustrates our capabilities, for ^{4}He the isovector model predicts a ratio of 1 [51], but others predict that nuclear effects change the d/u ratio and should therefore be observed here [50]. We will be able to explore any variation in bound nucleons with 1 to 2% statistical error bars – $i.e.$ 4% when including expected systematic error bars – from x_B of 0.1 to 0.5.

Summary and Answers to PAC44

Answers to PAC44 issues

Issues:

The Drift Chamber/scintillator technology needs to be demonstrated. We observe that a strong program of prototype studies is already underway.

Answer: We feel the technology has no major unknowns, wire chambers and scintillators have been used for decades as detectors of low energy nuclei and their properties have been well established. We present in the proposal a conceptual design demonstrating the feasibility of the detector, it is common practice to work on the optimization of a certain number of parameters after the proposal is approved. In particular, because it is easier to fund and man a project that has an approved status than a future proposal. Nevertheless, we remain open to discuss the topic in more depth if the committee has any concerns.

The TAC report voiced concerns about the length of the straw cell target and the substantial effort needed to integrate the DAQ for this detector into the CLAS12 DAQ.

Answer: The TAC and PAC44 raised concerns about the target cell. We have added extra discussion in section 2.3.3, which includes a table of existing or planned targets that are similar to the one we proposed. In summary, our proposed target is twice as wide as the ones used in the 6 GeV era for the BONuS and eg6 run and should therefore cause no issues. Note that the experiment 12-06-113 (BONuS12) is approved with a longer and thinner target. Their design will be reviewed by JLab for their experiment readiness review (ERR) before the PAC45 meeting. The result of this review should settle the question, but in any case, we propose a safer solution based on the successful experiments of the 6 GeV era.

The TAC and PAC44 raised issues regarding integration of ALERT into the CLAS12 DAQ. First, they raised a concern that the resources necessary for this integration are not

clearly identified. We have added text in section 2.6.3 outlining the resources provided by each group and the technical support they are expected to provide. Secondly, they mentioned a concern about the "substantial effort needed to integrate the DAQ for this detector into the CLAS12 DAQ". We want to emphasize that the read-out systems for ALERT are already being used in the CLAS12 DAQ to readout Micromegas detectors. Therefore, we will use and build on the experience gained from these systems.

The proposal does not clearly identify the resources (beyond generic JLAB/CLAS12 effort) necessary for DAQ integration which may be a substantial project.

Answer: As mentioned above, we do not feel this contribution is major, nevertheless we made this part clearer in the proposal.

During review the collaboration discovered an error in converting the luminosity to beam current. This resulted in a revision that will either require doubling the current or the target density. The beam current change would require changes to the Hall B beam dump, while raising the target density could impact the physics reach of the experiment by raising the minimum momentum threshold.

Answer: During the PAC44 proposal submission process the wrong beam current was requested. It was a factor of 2 too low. This increased beam current brought into contention the issue of possible Hall B beam current limits. We chose to use the higher beam current in this new version. Based on discussions with the Hall-B and accelerator staff, the only necessary upgrade necessary to run at $1\,\mu A$ is with the Hall-B beam blocker.

The precise interplay between final state interactions (FSI) and the tails of the initial state momentum distribution in DVCS on 4He was a topic of some debate. The collaboration makes an argument that the excellent acceptance of the apparatus allows novel constraints that allow selection of kinematic ranges where FSI is suppressed. While the originally suggested method to unambiguously identify areas of FSI was revised during the review, the committee remains unconvinced that the new kinematic selections suggested do not also cut into interesting regimes for the initial state kinematics. The committee believes that this is model dependent and would like to see more quantitative arguments than were provided in this version of the proposal.

Answer: We acknowledge there was an overstatement of the possibilities of the Tagged-DVCS proposal on this topic, this has been corrected. We now show a reduction, in opposition to the complete suppression previously claimed, in events that differ from the PWIA result. This finding is based on a simulation using a simple model of FSIs together with a Monte-Carlo event generator.

Summary:

The committee was generally enthusiastic about the diverse science program presented in this proposal; in particular the tagged EMC studies and the unique study of coherent GPD's on the 4He nucleus. However, the substantial modifications made in the proposal during review indicate that it could be substantially improved on a reasonably short time scale. We would welcome a new proposal that addresses the issues identified by the committee and by the collaboration.

Answer: We hope that the new proposals will answer all the questions raised by the PAC44 and will make the physics case even more compelling.

We also note that there are multiple experiments, proposed and approved, to study the EMC effect, including several with novel methods of studying the recoil system. We appreciate the comparisons of recoil technologies in this proposal and would welcome a broader physics discussion of how the proposed measurements contribute to a lab-wide strategy for exploring the EMC effect.

Answer: While no strategy document has been drafted after them, we want to point out to the PAC that the community of physicist interested by the partonic structure of nuclei meets regularly, with often a large focus on what can be done at JLab (see workshops at Trento[1], Miami[2], MIT[3], and Orsay[4] for example). Nonetheless, we added in the tagged EMC proposal summary an extension about the 12 GeV approved experiments related to the EMC effect. This short annex will hopefully clarify the context and the uniqueness of the present experiments.

Relation to other EMC related proposals

As noted by the PAC44, there is a wide program of experiments focused on the EMC effect that are already planned for the 12 GeV era of Jefferson Lab. We will try here to summarize this existing effort and explain why we think our approach is unique and essencial to a full understanding of the EMC effect.

The first, most obvious, class of experiments approved to study the EMC effect (experiments 12-10-008 and 12-10-103) are dedicated to its direct measurement in its traditional form, by measuring the inclusive ratio σ_A/σ_D. We note that these proposals concentrate on light nuclei, which is common with our proposal and many others. The motivation for this

---

[1]New Directions in Nuclear Deep Inelastic Scattering http://www.ectstar.eu/node/1221

[2]Next generation nuclear physics with JLab12 and EIC https://www.jlab.org/indico/event/121/

[3]Quantitative challenges in EMC and SRC Research and Data-Mining http://web.mit.edu/schmidta/www/src_workshop/

[4]Partons and Nuclei https://indico.in2p3.fr/event/14438/

choice is to look at nuclei which nuclear structure in term of nucleons is well understood to isolate partonic effects. These mesurements should provide high precision data allowing to understand the dependence of the EMC effect on local density and isospin symmetry.

Another approche is focused on deepening our understanding of the EMC effect (experiments 12-14-001 and 12-14-002) by measuring other inclusive observables like the spin structure functions or extracting the ratio $R = \sigma_L/\sigma_T$ in nuclei. These measurement will tell if the EMC effect is a general effect affecting similarly all structure functions or a more complex effect with different impact on these different observables. These are focused on very specific questions that once answered can have a major impact on our understanding of the EMC effect.

The short range correlations (SRC) approach is the focus of two EMC experiments (12-11-107 and 12-11-003A). These are exploring the link between SRC and the EMC effect in deuterium. This is motivated by the recent finding that the strength of the EMC effect seems correlated to the number of SRC pairs in a nucleus. A series of other experiments (12-06-105, 12-11-112 and 12-14-011) are focused specificly on SRC, while these can be partially motivated by the possible links to EMC, they do not address it directly. They probably should not be considered as part of the EMC program pursued in JLab.

Our proposal has a different approach to the EMC effect than all previously approved experiments. Our goal is to understand, in general, the link between the EMC effect and the internal nuclear dynamic using tagging. To achieve this goal, we decided to use two nuclear targets to compare the effect observed in different nuclei with similar spectator kinematics and in the same nuclei with different spectator kinematics. In our view this is necessary to ensure that we are really understanding the measured effect and we feel that a measurement on one of these targets only will always be subject to diverging interpretations. Also, we decided to focus on the mean field energies rather than high energies linked to SRC, but in a heavier helium nuclei. In this way we observe spectators of similar momentum classified SRC in deuterium but mean field in helium and can also assess if the effect depends purely on the momentum or other factors as well.

Summary and Beam Time Request

In summary, we proposed a tagged DIS measurement on light nuclear targets (^{2}H and ^{4}He) by detecting the backward recoiling spectators. By taking the advantage of the high luminosity and large kinematic coverage of CLAS12, we will be able to cover a wide range in spectator kinematic insuring a good control over FSI effects.

In order to make this measurement, we propose to use a new recoil detector to fit our experimental needs in term of low energy nuclei detection. The detector is designed such that it will provide good timing resolution and particle identification. Prototyping of this detector is currently underway in Orsay as part of a larger R&D program on drift chambers.

We propose to measure various tagged ratios and double ratios with their dependencies on the recoil kinematics. These measurements will provide very stringent tests of numerous models for the EMC and anti-shadowing effects and, more importantly, a model independent insight into the origin of the EMC effect in term of x_B or Q^2-rescaling.

In order to achieve all the goals presented in this proposal, we need 45 days of running. With 11 GeV electron beam at 3.10^{34} cm^{-2}s^{-1} (= 500 nA) with helium and deuterium targets (20 days each) and 5 days of commissioning of the ALERT detector at 2.2 GeV at various luminosities with helium and hydrogen targets.

Bibliography

[1] J. J. Aubert *et al.*, "The ratio of the nucleon structure functions $F2_n$ for iron and deuterium," *Phys. Lett.*, vol. B123, pp. 275–278, 1983.

[2] J. Ashman *et al.*, "Measurement of the Ratios of Deep Inelastic Muon - Nucleus Cross-Sections on Various Nuclei Compared to Deuterium," *Phys.Lett.*, vol. B202, p. 603, 1988.

[3] M. Arneodo *et al.*, "Shadowing in Deep Inelastic Muon Scattering from Nuclear Targets," *Phys.Lett.*, vol. B211, p. 493, 1988.

[4] M. Arneodo *et al.*, "Measurements of the nucleon structure function in the range $0.002 - \text{GeV}^2 < x < 0.17 - \text{GeV}^2$ and $0.2 - GeV^2 < q^2 < 8 - GeV^2$ in deuterium, carbon and calcium," *Nucl.Phys.*, vol. B333, p. 1, 1990.

[5] J. Gomez *et al.*, "Measurement of the A-dependence of deep inelastic electron scattering," *Phys.Rev.*, vol. D49, pp. 4348–4372, 1994.

[6] D. Allasia *et al.*, "Measurement of the neutron and the proton F2 structure function ratio," *Phys.Lett.*, vol. B249, pp. 366–372, 1990.

[7] J. Seely *et al.*, "New measurements of the EMC effect in very light nuclei," *Phys. Rev. Lett.*, vol. 103, p. 202301, 2009.

[8] D. F. Geesaman, K. Saito, and A. W. Thomas, "The nuclear EMC effect," *Ann. Rev. Nucl. Part. Sci.*, vol. 45, pp. 337–390, 1995.

[9] P. R. Norton, "The EMC effect," *Rept. Prog. Phys.*, vol. 66, pp. 1253–1297, 2003.

[10] S. Malace, D. Gaskell, D. W. Higinbotham, and I. Cloet, "The Challenge of the EMC Effect: existing data and future directions," *Int.J.Mod.Phys.*, vol. E23, p. 1430013, 2014.

[11] M. Ericson and A. W. Thomas, "Pionic Corrections and the EMC Enhancement of the Sea in Iron," *Phys. Lett.*, vol. B128, p. 112, 1983.

[12] G. V. Dunne and A. W. Thomas, "DEEP INELASTIC SCATTERING AS A PROBE OF NUCLEON AND NUCLEAR STRUCTURE," *Nucl. Phys.*, vol. A446, pp. 437c–443c, 1985.

[13] S. V. Akulinichev, S. A. Kulagin, and G. M. Vagradov, "The Role of Nuclear Binding in Deep Inelastic Lepton Nucleon Scattering," *Phys. Lett.*, vol. B158, pp. 485–488, 1985.

[14] H. Jung and G. A. Miller, "NUCLEONIC CONTRIBUTION TO LEPTON NUCLEUS DEEP INELASTIC SCATTERING," *Phys. Lett.*, vol. B200, pp. 351–356, 1988.

[15] F. E. Close, R. G. Roberts, and G. G. Ross, "The Effect of Confinement Size on Nuclear Structure Functions," *Phys. Lett.*, vol. B129, p. 346, 1983.

[16] O. Nachtmann and H. J. Pirner, "Color Conductivity in Nuclei and the EMC Effect," *Z. Phys.*, vol. C21, p. 277, 1984.

[17] R. L. Jaffe, F. E. Close, R. G. Roberts, and G. G. Ross, "On the Nuclear Dependence of Electroproduction," *Phys. Lett.*, vol. B134, p. 449, 1984.

[18] F. E. Close, R. G. Roberts, and G. G. Ross, "Factorization Scale Independence, the Connection between Alternative Explanations of the EMC Effect and QCD Predictions for Nuclear Properties," *Nucl. Phys.*, vol. B296, p. 582, 1988.

[19] L. Frankfurt and M. Strikman, "POINT - LIKE CONFIGURATIONS IN HADRONS AND NUCLEI AND DEEP INELASTIC REACTIONS WITH LEPTONS: EMC AND EMC LIKE EFFECTS," *Nucl.Phys.*, vol. B250, pp. 143–176, 1985.

[20] L. Frankfurt and M. Strikman, "High-Energy Phenomena, Short Range Nuclear Structure and QCD," *Phys.Rept.*, vol. 76, pp. 215–347, 1981.

[21] S. Kumano and F. E. Close, "DEPENDENCE OF THE EMC EFFECT ON NUCLEAR STRUCTURE," *Phys. Rev.*, vol. C41, pp. 1855–1858, 1990.

[22] C. Ciofi degli Atti and S. Liuti, "Can nuclear binding explain the classical EMC effect?," *Nucl.Phys.*, vol. A532, pp. 241–248, 1991.

[23] C. Ciofi degli Atti, L. P. Kaptari, and S. Scopetta, "Semi-inclusive deep inelastic lepton scattering off complex nuclei," *Eur. Phys. J.*, vol. A5, pp. 191–207, 1999.

[24] D. Higinbotham, J. Gomez, and E. Piasetzky, "Nuclear Scaling and the EMC Effect," 2010.

[25] L. Weinstein *et al.*, "Short Range Correlations and the EMC Effect," *Phys.Rev.Lett.*, vol. 106, p. 052301, 2011.

[26] A. Aprahamian *et al.*, "Reaching for the horizon: The 2015 long range plan for nuclear science," 2015.

[27] L. Frankfurt, M. Strikman, D. Day, and M. Sargsian, "Evidence for short range correlations from high Q**2 (e, e-prime) reactions," *Phys.Rev.*, vol. C48, pp. 2451–2461, 1993.

[28] K. Egiyan *et al.*, "Observation of nuclear scaling in the A(e, e-prime) reaction at x(B) greater than 1," *Phys.Rev.*, vol. C68, p. 014313, 2003.

[29] K. Egiyan *et al.*, "Measurement of 2- and 3-nucleon short range correlation probabilities in nuclei," *Phys.Rev.Lett.*, vol. 96, p. 082501, 2006.

[30] O. Hen *et al.*, "Momentum sharing in imbalanced Fermi systems," *Science*, vol. 346, pp. 614–617, 2014.

[31] C. Ciofi degli Atti *et al.*, "On the dependence of the wave function of a bound nucleon on its momentum and the EMC effect," *Phys. Rev.*, vol. C76, p. 055206, 2007.

[32] N. Baillie *et al.*, "Measurement of the neutron F2 structure function via spectator tagging with CLAS," *Phys.Rev.Lett.*, vol. 108, p. 142001, 2012.

[33] M. Hattawy *et al.* (EG6 Working Group), "Deeply Virtual Compton Scattering off ^{4}He," *CLAS internal analysis note*, 2016.

[34] C. Ciofi degli Atti and B. Z. Kopeliovich, "Final state interaction in semi-inclusive DIS off nuclei," *Eur. Phys. J.*, vol. A17, pp. 133–144, 2003.

[35] C. Ciofi degli Atti, L. Kaptari, and B. Kopeliovich, "Final state interaction effects in semiinclusive DIS off the deuteron," *Eur.Phys.J.*, vol. A19, pp. 145–151, 2004.

[36] M. Alvioli, C. Ciofi degli Atti, and V. Palli, "Slow proton production in semi-inclusive DIS off nuclei: The Role of final state interaction," *Nucl.Phys.*, vol. A782, pp. 175–178, 2007.

[37] V. Palli *et al.*, "Slow Proton Production in Semi-Inclusive Deep Inelastic Scattering off Deuteron and Complex Nuclei: Hadronization and Final State Interaction Effects," *Phys.Rev.*, vol. C80, p. 054610, 2009.

[38] L. Frankfurt and M. Strikman, "Hard Nuclear Processes and Microscopic Nuclear Structure," *Phys.Rept.*, vol. 160, pp. 235–427, 1988.

[39] C. Ciofi degli Atti and S. Simula, "Slow proton production in semiinclusive deep inelastic lepton scattering off nuclei," *Phys.Lett.*, vol. B319, pp. 23–28, 1993.

[40] W. Melnitchouk, M. Sargsian, and M. I. Strikman, "Probing the origin of the EMC effect via tagged structure functions of the deuteron," *Z. Phys.*, vol. A359, pp. 99–109, 1997.

[41] C. Ciofi delgi Atti and L. Kaptari, "A Non factorized calculation of the process He-3(e,e-prime p) H-2 at medium energies," *Phys.Rev.Lett.*, vol. 100, p. 122301, 2008.

[42] C. Ciofi degli Atti and L. Kaptari, "Semi-inclusive Deep Inelastic Scattering off Few-Nucleon Systems: Tagging the EMC Effect and Hadronization Mechanisms with Detection of Slow Recoiling Nuclei," *Phys.Rev.*, vol. C83, p. 044602, 2011.

[43] W. Melnitchouk, A. W. Schreiber, and A. W. Thomas, "Deep inelastic scattering from off-shell nucleons," *Phys. Rev.*, vol. D49, pp. 1183–1198, 1994.

[44] A. Klimenko *et al.*, "Electron scattering from high-momentum neutrons in deuterium," *Phys.Rev.*, vol. C73, p. 035212, 2006.

[45] L. P. Kaptari, A. Del Dotto, E. Pace, G. Salme', and S. Scopetta, "Distorted spin-dependent spectral function of an A=3 nucleus and semi-inclusive deep inelastic scattering processes," *Phys. Rev.*, vol. C89, no. 3, p. 035206, 2014.

[46] K. A. Griffioen *et al.*, "Measurement of the EMC Effect in the Deuteron," *Phys. Rev.*, vol. C92, no. 1, p. 015211, 2015.

[47] H. Fenker *et al.*, "BoNus: Development and use of a radial TPC using cylindrical GEMs," *Nucl. Instrum. Meth.*, vol. A592, pp. 273–286, 2008.

[48] M. Sargsian and M. Strikman, "Model independent method for determination of the DIS structure of free neutron," *Phys. Lett.*, vol. B639, pp. 223–231, 2006.

[49] W. Cosyn, V. Guzey, M. Sargsian, M. Strikman, and C. Weiss, "Electron-deuteron DIS with spectator tagging at EIC: Development of theoretical framework," *EPJ Web Conf.*, vol. 112, p. 01022, 2016.

[50] S. J. Brodsky, I. Schmidt, and J.-J. Yang, "Nuclear antishadowing in neutrino deep inelastic scattering," *Phys. Rev.*, vol. D70, p. 116003, 2004.

[51] I. C. Cloet, W. Bentz, and A. W. Thomas, "Isovector EMC effect explains the NuTeV anomaly," *Phys. Rev. Lett.*, vol. 102, p. 252301, 2009.

[52] "CLAS12 Technical Design Report," 2008.

[53] M. Amaryan *et al.*, "The Structure of the Free Neutron at Large x-Bjorken (PR12-06-113)," *A proposal to PAC 30*, 2006.

[54] J. Peyré, B. Genolini, and J. Poutas, "A Full-Scale Prototype for the Tracking Chambers of the ALICE Muon Spectrometer," 1998.

[55] T. Abe *et al.*, "Belle II Technical Design Report," 2010.

[56] E. Etzion *et al.*, "The Certification of ATLAS Thin Gap Chambers Produced in Israel and China," 2004.

[57] S. Biagi, "Monte Carlo simulation of electron drift and diffusion in counting gases under the influence of electric and magnetic fields," *Nucl.Instrum.Meth.*, vol. A421, pp. 234–240, 1999.

[58] C. Ciofi degli Atti *et al.*, "The readout system for the clas12 micromegas vertex tracker," in *2014 19th IEEE-NPSS Real Time Conference*, pp. 1–11, May 2014.

[59] T. C. Collaboration, "Clas12 forward tagger (ft) technical design report." `https://www.jlab.org/Hall-B/clas12-web/docs/ft-tdr.2.0.pdf`, 2012. Online; accessed 29 January 2016.

[60] "Petiroc-2a." `http://www.weeroc.com/en/products/petiroc-2`. Accessed: 2017-05-15.

[61] C. Zorn, "A pedestrian's guide to radiation damage in plastic scintillators," *Nucl. Phys. Proc. Suppl.*, vol. 32, pp. 377–383, 1993.

[62] Y. Qiang, C. Zorn, F. Barbosa, and E. Smith, "Radiation Hardness Tests of SiPMs for the JLab Hall D Barrel Calorimeter," *Nucl. Instrum. Meth.*, vol. A698, pp. 234–241, 2013.

[63] Y. Qiang, C. Zorn, F. Barbosa, and E. Smith, "Neutron radiation hardness tests of SiPMs," *AIP Conf. Proc.*, vol. 1560, pp. 703–705, 2013.

[64] S. Ahmad. Private communication, May 2017. Weeroc SAS.

[65] K. Emi *et al.*, "Study of a dE/ dx measurement and the gas-gain saturation by a prototype drift chamber for the BELLE-CDC," *Nucl. Instrum. Meth.*, vol. A379, pp. 225–231, 1996.

[66] S. Stepanyan and A. P. Freyberger. Private communication, May 2017.

[67] R. B. Wiringa, V. Stoks, and R. Schiavilla, "An Accurate nucleon-nucleon potential with charge independence breaking," *Phys.Rev.*, vol. C51, pp. 38–51, 1995.

[68] B. S. Pudliner *et al.*, "Quantum Monte Carlo calculations of nuclei with A ¡= 7," *Phys.Rev.*, vol. C56, pp. 1720–1750, 1997.

[69] R. B. Wiringa , *Private communication.*

[70] R. Duprã©, *Quark Fragmentation and Hadron Formation in Nuclear Matter.* PhD thesis, Lyon, IPN, 2011.

[71] C. Ciofi degli Atti , *Private communication.*

[72] W. Cosyn and M. Sargsian, "Final-state interactions in semi-inclusive deep inelastic scattering off the Deuteron," *Phys. Rev.*, vol. C84, p. 014601, 2011.

[73] K. Egiian, L. Frankfurt, W. R. Greenberg, G. A. Miller, M. Sargsian, and M. Strikman, "Searching for color coherent effects at intermediate Q**2 via double scattering processes," *Nucl. Phys.*, vol. A580, pp. 365–382, 1994.

[74] L. L. Frankfurt, W. R. Greenberg, G. A. Miller, M. M. Sargsian, and M. I. Strikman, "Color transparency effects in electron deuteron interactions at intermediate Q**2," *Z. Phys.*, vol. A352, pp. 97–113, 1995.

[75] S. Scopetta , *Private communication.*